International Journal of Solids and Structures 50 (2013) 907–919

Contents lists available at SciVerse ScienceDirect

International Journal of Solids and Structures

journal homepage: www.elsevier.com/locate/ijsolstr

A new and general formulation of the parametric HFGMC micromechanical method for two and three-dimensional multi-phase composites

Rami Haj-Ali [a,b,*], Jacob Aboudi [a]

[a] School of Mechanical Engineering, Faculty of Engineering, Tel-Aviv University, Ramat-Aviv 69978, Israel
[b] Georgia Institute of Technology, Atlanta, GA 30332, USA

ARTICLE INFO

Article history:
Received 30 April 2012
Received in revised form 29 October 2012
Available online 5 December 2012

Keywords:
High fidelity generalized method of cells
HFGMC
Multiphase composites
Arbitrary geometry
Micromechanics
Unit-cell

ABSTRACT

The recent two-dimensional (2D) parametric formulation of the *high fidelity generalized method of cells* (HFGMC) reported by the authors is generalized for the micromechanical analysis of three-dimensional (3D) multiphase composites with periodic microstructure. Arbitrary hexahedral subcell geometry is developed to discretize a triply periodic repeating unit-cell (RUC). Linear parametric-geometric mapping is employed to transform the arbitrary hexahedral subcell shapes from the physical space to an auxiliary orthogonal shape, where a complete quadratic displacement expansion is performed. Previously in the 2D case, additional three equations are needed in the form of average moments of equilibrium as a result of the inclusion of the bilinear terms. However, the present 3D parametric HFGMC formulation eliminates the need for such additional equations. This is achieved by expressing the coefficients of the full quadratic polynomial expansion of the subcell in terms of the side or face average-displacement vectors. The 2D parametric and orthogonal HFGMC are special cases of the present 3D formulation. The continuity of displacements and tractions, as well as the equilibrium equations, are imposed in the average (integral) sense as in the original HFGMC formulation. Each of the six sides (faces) of a subcell has an independent average displacement micro-variable vector which forms an energy-conjugate pair with the transformed average-traction vector. This allows generating symmetric stiffness matrices along with internal resisting vectors for the subcells which enhances the computational efficiency. The established new parametric 3D HFGMC equations are formulated and solution implementations are addressed. Several applications for triply periodic 3D composites are presented to demonstrate the general capability and varsity of the present parametric HFGMC method for refined micromechanical analysis by generating the spatial distributions of local stress fields. These applications include triply periodic composites with inclusions in the form of a cavity, spherical inclusion, ellipsoidal inclusion, and discontinuous aligned short fiber. A 3D repeating unit-cell for foam material composite is simulated.

1. Introduction

Early analytical three-dimensional micromechanical models have been concerned with homogenization methods able to generate the effective elastic properties of composites. A classical approach employs the Eshelby (1957) single inclusion elasticity solution in a homogenization scheme, e.g. the self consistent scheme and its generalizations, Christensen (1979), and Mori and Tanaka (1973) methods. The latter approach has been widely used in the literature and extensions from single to double or nested inclusions have been reported, e.g. Hori and Nemat-Nasser (1993). Highlights of further extensions to compute the effective viscoelastic and inelastic composites has been given by Wang and Weng (1992) and Gavazzi and Lagoudas (1990), for example. Additional extensions to composites with inelastic matrix and progressive failure including debonding have been proposed by Ju and Tseng (1996). The latter models have been generalized by Ju and Sun (2001) to develop a 3D statistical micromechanical damage modeling framework for multiphase brittle composites with combinations of interacting microcracks and inclusions. Finally, combined damage 3D micromechanics have been formulated and applied to functionally graded materials by Paulino et al. (2006).

A different 3D micromechanics approach is to use discrete based subvolumes where expansion of the displacement is carried out in order to capture the local fields. To this end, the classical displacement-based nonlinear FE method has been widely utilized, e.g. Levy and Papazian (1990). Jain and Ghosh (2008, 2009) used an extension from their 2D to 3D microstructural RVE model with

* Corresponding author at: School of Mechanical Engineering, Faculty of Engineering, Tel-Aviv University, Ramat-Aviv 69978, Israel. Tel.: +972 3 640 8207; fax: +972 3 640 7617.
E-mail address: rami98@eng.tau.ac.il (R. Haj-Ali).

0020-7683/$ - see front matter © 2012 Elsevier Ltd. All rights reserved.
http://dx.doi.org/10.1016/j.ijsolstr.2012.11.009

Voronoi cell elements including damage. Multi-level variational formulation has been achieved to construct 3D micromechanics with and without damage, e.g. Fish et al. (1999). Finally the previous micromodels and other simplified 3D micromechanics have been used for local–global structural analysis. Towards that end, the lower-order GMC has been developed for 3D composites. Thus, Haj-Ali et al. (2001) developed a nested 3D micromodels for nonlinear multi-scale pultruded composite structures. Muliana and Kim (2007) employed a simplified 3D micromodel using relatively small number of subcells for the viscoelastic multi-scale analysis of composite structures. The GMC has been utilized by Pahr and Arnold (2002) for the analysis of metal matrix composites with discontinuous fibers, by Bednarcyk and Arnold (2003) for the modeling of woven composites, and by Liu et al. (2011) for a multiscale analysis of triaxially braided composites. The higher-order regular orthogonal 3D-HFGMC has been employed by Bednarcyk et al. (2008) in their investigation of the foam insulation of the space shuttle.

Refined micromechanics is a class of nonlinear micromechanical models capable not only to predict the instantaneous effective stiffness of a periodic heterogeneous medium, but also to accurately predict the local spatial distributions of the deformations within the repeating unit-cell (RUC). The latter requirement is needed in order to use such modeling for nonlinear material response along with potential localized damage, e.g. microcracking, fiber–matrix interface debonding, material defects and imperfections, among other modes.

The HFGMC method is a higher-order refined micromechanical theory and has evolved from its lower-order predecessors, the method of cells (MOC) (Aboudi, 1982, 1991), and the generalized method of cells (GMC) (Paley and Aboudi, 1992), respectively. The HFGMC micromechanical model is well suited for detailed nonlinear analysis of multiphase composites, Aboudi (2004). Unlike general classical numerical methods such as finite element (FE) and finite-volume (FV), the HFGMC is tailored and specialized to micromechanics of periodic composites. It is explicitly based on micromechanical variables needed to establish the elastic and inelastic concentration tensors of the phases in addition to the detailed local fields. The formulation of the HFGMC is performed using average equilibrium, traction and displacement continuity equations. This is because it aims to strike a balance between simplicity and accuracy without the need for excessive number of discrete sub-volumes (subcells). The computational affordability is especially important when HFGMC is integrated within a nonlinear analysis of composite structures including localized effects, often called multi-scale or local–global modeling.

Several applications and implementations of the HFGMC have been performed to model different physical effects in periodic composites, such as coupled electro-magneto-thermo-elastic (Aboudi, 2001), viscoelastic-viscoplastic micromechanics (Aboudi et al., 2002, 2003; Aboudi, 2005), bond damage of fiber (Bednarcyk et al., 2004; Ryvkin and Aboudi, 2007). A review of the method and application for HFGMC applied to smart materials can be found in Aboudi (2007) and Aboudi and Freed (2010). Damage evolution effects have been introduced within HFGMC by Haj-Ali and Aboudi (2009), Bednarcyk et al. (2010) and Aboudi (2011). These include cohesive growth between the subcells, cell extinction damage (CED), isotropic and anisotropic damage evolutions in unidirectional composites. A comprehensive recent reference to the HFGMC method with wide range of applications can be found in Aboudi et al. (2013).

The original HFGMC formulations have been performed in conjunction with orthogonal array of subcells used to depict the geometry of the phases (regular array). This limitation requires a relatively large number of subcells if the objective is to accurately capture refined geometrical features and the spatial variations of the local solution fields. Despite this limitation, the previous applications have demonstrated the effectiveness of the method to generate the local solution fields by using sufficiently large number of rectangular subcells. It should be emphasized that few number of rectangular subcells is sufficient to generate the effective linear and nonlinear response for the overall composite with high accuracy. In fact, this is one of the advantages of using the HFGMC in a local–global analysis of composite structures with selective geometrical refinement for the microstructure (Haj-Ali and Aboudi, 2009).

A natural extension that overcomes the limitations of the regular orthogonal array is to employ a parametric mapping. To this end, Haj-Ali and Aboudi (2010) used linear geometrical mapping of the subcells to map the geometry of the phases of the composite. This linear and parametric geometric mapping can be applied for a unit-cell with general phase geometry using arbitrary quadrilateral cell shapes that are transformed to an auxiliary uniform square shape (natural coordinates). It is important to note that while the geometric mapping is linear, the subcell displacement expansion is of a full quadratic form (subparametric). In addition, the complete form of the Jacobian transformation has been employed without approximation which necessitates a numerical integration of the HFGMC equations. The utilization of a full quadratic expansion vector with its bilinear terms in a subcell required three additional equations which were chosen as the average moment of the equilibrium equations. It was emphasized by authors that this choice is not optimal and further research is needed to reach a proper form of the needed relations.

In the present investigation, a generalization of the parametric HFGMC to 3D multiphase composites with periodic microstructure is offered. To this end, general hexahedral subcells are introduced to model triply-periodic composites. Here too, the full quadratic displacement expansion is still used within the parametric HFGMC. However, we now show that the average displacement vectors at the edges (or faces) of the subcell can be expressed in terms of the coefficients of the expansion to form an independent subset of side-based variables. Furthermore, it is shown that corresponding transformed average-traction at the edges are conjugate pairs to the average displacements. In this way, two outcomes can be achieved. In the first, relations for the bilinear terms can be established with the quadratic coefficients of the displacements and thus no need for additional moment of equilibrium relations. In the second outcome, the energy conjugate pair result in symmetric linearized form of the overall HFGMC equations with obvious computational advantages. The present new 3D parametric HFGMC generalization allows the analysis of composites with general shape of inclusions. The 2D parametric HFGMC can be obtained as a special case of the present formulation.

This paper is organized as follows. In Section 2, the general theory to 3D parametric HFGMC is presented including the 2D-HFGMC as a special case. In Section 3, computational implementation aspects are described and discussed. Wide range of applications are given in the next Section, followed by concluding remarks.

2. General formulation

The HFGMC micromechanical method is presently extended for general parametric formulation suitable for three-dimensional (3D) analysis of multiphase composite materials. Fig. 1 schematically illustrates a triply-periodic multiphase material system having a global coordinates (x_1, x_2, x_3). The repeating unit cell (RUC) of this periodic composite can be identified and described by using the coordinate system (y_1, y_2, y_3). The goals of the HFGMC micromechanical method, based on the homogenization technique for periodic composites, are to predict the overall effective properties as well as the spatial local deformation fields. In

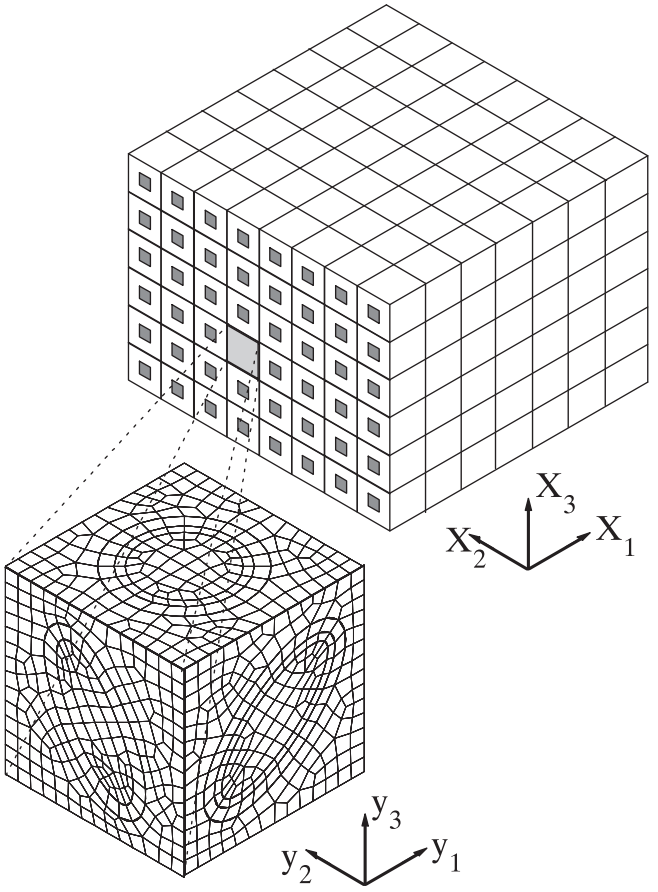

Fig. 1. Schematic illustration of a triply periodic array in the global (x_1, x_2, x_3) space of multiphase composite media with its repeating unit-cell (RUC) having hexahedral subcells, defined with respect to its (y_1, y_2, y_3) local coordinate system.

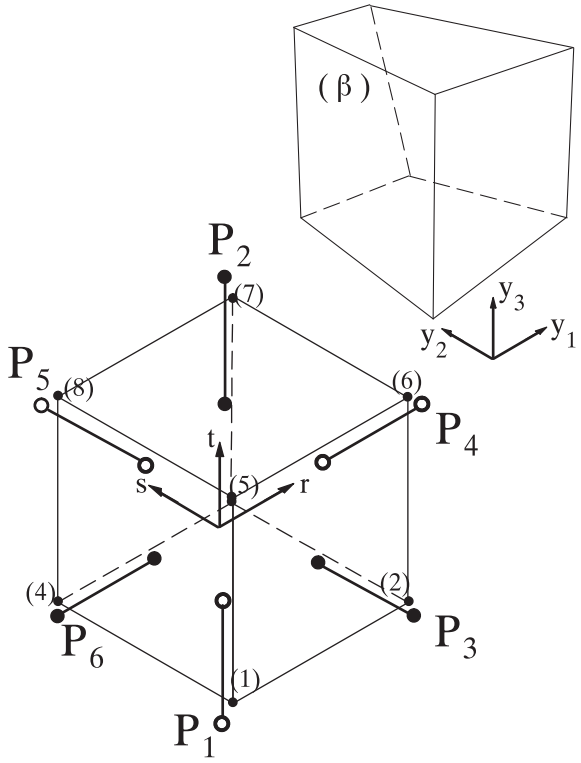

Fig. 2. A hexahedral shaped subcell in its physical and natural coordinates. Numbering for the faces and corners are shown.

the HFGMC framework, the RUC is divided into array of cells, often denoted as subcells. In the present section, this method is extended to analyze an RUC of a triply-periodic composite with irregular array of generally shaped hexahedral subcells. Fig. 1 shows a schematic RUC domain which is discretized into a general assembly of hexahedral subcells to represent the different phase geometries. Fig. 2 shows a general hexahedral subcell isolated and shown in its physical coordinates (y_1, y_2, y_3). This subcell is mapped to a uniform parametric coordinate system (r, s, t) using the classical linear transformation

$$y_i(r,s,t) = \sum_{k=1}^{8} H_k(r,s,t) y_{ki}, \quad i = 1,2,3 \tag{1}$$

where y_i, $i = 1,2,3$, are the coordinates of a general point within the subcell (β) mapped from the parent parametric coordinates to the physical RUC coordinates, and

$$\begin{aligned}
H_1 &= \frac{1}{8}(1-r)(1-s)(1-t), \quad H_5 = \frac{1}{8}(1-r)(1-s)(1+t)\\
H_2 &= \frac{1}{8}(1+r)(1-s)(1-t), \quad H_6 = \frac{1}{8}(1+r)(1-s)(1+t)\\
H_3 &= \frac{1}{8}(1+r)(1+s)(1-t), \quad H_7 = \frac{1}{8}(1+r)(1+s)(1+t)\\
H_4 &= \frac{1}{8}(1-r)(1+s)(1-t), \quad H_8 = \frac{1}{8}(1-r)(1+s)(1+t)
\end{aligned} \tag{2}$$

and y_{ki} are the corner coordinates of the subcell.

In the present 3D HFGMC formulation, the complete quadratic form of the displacement expansion in the subcell, is given by

$$\begin{aligned}
\mathbf{u} = {} & \boldsymbol{\epsilon}^0 \cdot \mathbf{x} + \mathbf{W}_{000} + \mathbf{W}_{100} r + \mathbf{W}_{010} s + \mathbf{W}_{001} t + \mathbf{W}_{110} rs + \mathbf{W}_{101} rt \\
& + \mathbf{W}_{011} st + \frac{1}{2}\mathbf{W}_{200}(3r^2 - 1) \\
& + \frac{1}{2}\mathbf{W}_{020}(3s^2 - 1) + \frac{1}{2}\mathbf{W}_{002}(3t^2 - 1)
\end{aligned} \tag{3}$$

where the applied remote global-scale displacement field is given by $\mathbf{u}^0 \equiv \boldsymbol{\epsilon}^0 \cdot \mathbf{x}$. This expansion is a direct extension of the full quadratic expansion which has been used by Haj-Ali and Aboudi (2010) in the case of the parametric HFGMC for doubly-periodic composites. However, in the present parametric formulation, the mixed bilinear terms of this expansion are shown to be dependent variables. This resolves the open question that has been raised by Haj-Ali and Aboudi (2010) on the optimal method that should be used to determine these terms. Previously, the bilinear terms have treated as independent variables and consequently additional moment of equilibrium equations should have introduce to determine them. To this end, let us define the average displacement vector on the six faces of the hexahedral subcell:

$$\bar{\boldsymbol{u}}^{(\beta_k)} = \frac{1}{A_k}\int_{A_k} \boldsymbol{u}^{(\beta)}(\boldsymbol{y}) dA_k = \frac{1}{4}\int_{-1}^{1}\int_{-1}^{1} \boldsymbol{u}^{(\beta)}(\xi_k, \eta_k) d\xi_k d\eta_k, \quad k = 1,2,\ldots,6 \tag{4}$$

where (ξ_k, η_k) are the surface parametric integration variables of the kth edge or face of the subcell denoted by (β_k). The above integration provides the six vectors of the surface-average displacements expressed in terms of the expansion coefficients $\boldsymbol{W}_{(lmn)}$ as follows:

$$\begin{Bmatrix} \bar{\boldsymbol{u}}^{(\beta_1)} \\ \bar{\boldsymbol{u}}^{(\beta_2)} \\ \bar{\boldsymbol{u}}^{(\beta_3)} \\ \bar{\boldsymbol{u}}^{(\beta_4)} \\ \bar{\boldsymbol{u}}^{(\beta_5)} \\ \bar{\boldsymbol{u}}^{(\beta_6)} \\ \boldsymbol{W}_{000} \end{Bmatrix} - \begin{Bmatrix} \bar{\boldsymbol{u}}^{0,(\beta_1)} \\ \bar{\boldsymbol{u}}^{0,(\beta_2)} \\ \bar{\boldsymbol{u}}^{0,(\beta_3)} \\ \bar{\boldsymbol{u}}^{0,(\beta_4)} \\ \bar{\boldsymbol{u}}^{0,(\beta_5)} \\ \bar{\boldsymbol{u}}^{0,(\beta_6)} \\ \boldsymbol{0} \end{Bmatrix} \equiv \begin{Bmatrix} \boldsymbol{W}_1 \\ \boldsymbol{W}_2 \\ \boldsymbol{W}_3 \\ \boldsymbol{W}_4 \\ \boldsymbol{W}_5 \\ \boldsymbol{W}_6 \\ \boldsymbol{W}_0 \end{Bmatrix} = \begin{bmatrix} 0 & 0 & -1 & 0 & 0 & 1 & 1 \\ 0 & 0 & 1 & 0 & 0 & 1 & 1 \\ 0 & -1 & 0 & 0 & 1 & 0 & 1 \\ 1 & 0 & 0 & 1 & 0 & 0 & 1 \\ 0 & 1 & 0 & 0 & 1 & 0 & 1 \\ -1 & 0 & 0 & 1 & 0 & 0 & 1 \\ 0 & 0 & 0 & 0 & 0 & 0 & 1 \end{bmatrix} \begin{Bmatrix} \boldsymbol{W}_{100} \\ \boldsymbol{W}_{010} \\ \boldsymbol{W}_{001} \\ \boldsymbol{W}_{200} \\ \boldsymbol{W}_{020} \\ \boldsymbol{W}_{002} \\ \boldsymbol{W}_{000} \end{Bmatrix} \tag{5}$$

The inverse relation of Eq. (5) is given by:

$$\begin{Bmatrix} \boldsymbol{W}_{100} \\ \boldsymbol{W}_{010} \\ \boldsymbol{W}_{001} \\ \boldsymbol{W}_{200} \\ \boldsymbol{W}_{020} \\ \boldsymbol{W}_{002} \\ \boldsymbol{W}_{000} \end{Bmatrix} = \frac{1}{2} \begin{bmatrix} 0 & 0 & 0 & 1 & 0 & -1 & 0 \\ 0 & 0 & -1 & 0 & 1 & 0 & 0 \\ -1 & 1 & 0 & 0 & 0 & 0 & 0 \\ 0 & 0 & 0 & 1 & 0 & 1 & -2 \\ 0 & 0 & 1 & 0 & 1 & 0 & -2 \\ 1 & 1 & 0 & 0 & 0 & 0 & -2 \\ 0 & 0 & 0 & 0 & 0 & 0 & 2 \end{bmatrix} \begin{Bmatrix} \boldsymbol{W}_1 \\ \boldsymbol{W}_2 \\ \boldsymbol{W}_3 \\ \boldsymbol{W}_4 \\ \boldsymbol{W}_5 \\ \boldsymbol{W}_6 \\ \boldsymbol{W}_0 \end{Bmatrix} \tag{6}$$

It can be readily observed that the bilinear coefficients $\boldsymbol{W}_{110}$, $\boldsymbol{W}_{101}$, $\boldsymbol{W}_{011}$ do not contribute to the average displacements. Thus it is possible to assume that these are dependent coefficients if our aim is to use the average displacements as the primary independent variables. Hence, two possible solutions can be identified. The first trivial case is to assume that the bilinear terms to be zero:

$$\boldsymbol{W}_{110} = \boldsymbol{W}_{011} = \boldsymbol{W}_{101} = \boldsymbol{0} \tag{7}$$

This solution generates a truncated quadratic expansion that may affect the spatial distribution of the elastic fields. However, the average strain in the subcell, directly responsible for the overall elastic effective stiffness of the RUC, is not affected due to the vanishing integration of the bilinear terms in the hexahedral domain.

Alternatively, a non-trivial solution can be obtained while retaining the complete quadratic expansion (3), maintaining terms' symmetry and frame indifference of this polynomial form. Here

$$\begin{aligned} \boldsymbol{W}_{110} &= \frac{1}{2}(\boldsymbol{W}_{200} + \boldsymbol{W}_{020}) = \frac{1}{4}(\boldsymbol{W}_3 + \boldsymbol{W}_4 + \boldsymbol{W}_5 + \boldsymbol{W}_6 - 4\boldsymbol{W}_0) \\ \boldsymbol{W}_{011} &= \frac{1}{2}(\boldsymbol{W}_{020} + \boldsymbol{W}_{002}) = \frac{1}{4}(\boldsymbol{W}_1 + \boldsymbol{W}_2 + \boldsymbol{W}_3 + \boldsymbol{W}_5 - 4\boldsymbol{W}_0) \\ \boldsymbol{W}_{101} &= \frac{1}{2}(\boldsymbol{W}_{200} + \boldsymbol{W}_{002}) = \frac{1}{4}(\boldsymbol{W}_1 + \boldsymbol{W}_2 + \boldsymbol{W}_4 + \boldsymbol{W}_6 - 4\boldsymbol{W}_0) \end{aligned} \tag{8}$$

It can be verified that the average displacement relations given by Eq. (5) are maintained with the trivial and the non-trivial forms given for the bilinear terms, Eqs. (7) and (8), respectively. Eq. (8) can be considered as unique if the objective is to link the mixed bilinear coefficients with the higher order ones and yet maintain the average displacement relations with terms' symmetry and frame indifference. It should be noted that the trivial case is a direct result of the original HFGMC formulation, e.g. Aboudi (2004), for orthogonal and regular array of subcells where both physical and natural coordinates coincide and the Jacobian of the mapping is constant. As a result of the above derivations it is possible to rewrite the displacement expansion (3) in the following compact form:

$$\begin{aligned} \mathbf{u} = {} & \boldsymbol{\epsilon}^0 \cdot \mathbf{x} + \mathbf{W}_0 + \frac{1}{2}(\boldsymbol{W}_4 - \boldsymbol{W}_6)r + \frac{1}{2}(\boldsymbol{W}_5 - \boldsymbol{W}_3)s \\ & + \frac{1}{2}(\boldsymbol{W}_2 - \boldsymbol{W}_1)t \\ & + \frac{1}{4}(\boldsymbol{W}_4 + \boldsymbol{W}_6 - 2\boldsymbol{W}_0)\left(3r^2 + rs + rt - 1\right) \\ & + \frac{1}{4}(\boldsymbol{W}_3 + \boldsymbol{W}_5 - 2\boldsymbol{W}_0)\left(3s^2 + rs + st - 1\right) \\ & + \frac{1}{4}(\boldsymbol{W}_1 + \boldsymbol{W}_2 - 2\boldsymbol{W}_0)\left(3t^2 + rt + st - 1\right) \end{aligned} \tag{9}$$

It is worth mentioning that in the special case of 2D parametric HFGMC for doubly-periodic composites, the above expansion takes the form:

$$\begin{aligned} \mathbf{u} = {} & \boldsymbol{\epsilon}^0 \cdot \mathbf{x} + \mathbf{W}_0 + \frac{1}{2}(\boldsymbol{W}_4 - \boldsymbol{W}_6)r + \frac{1}{2}(\boldsymbol{W}_5 - \boldsymbol{W}_3)s \\ & + \frac{1}{4}(\boldsymbol{W}_4 + \boldsymbol{W}_6 - 2\boldsymbol{W}_0)\left(3r^2 + rs - 1\right) \\ & + \frac{1}{4}(\boldsymbol{W}_3 + \boldsymbol{W}_5 - 2\boldsymbol{W}_0)\left(3s^2 + rs - 1\right) \end{aligned} \tag{10}$$

where $\boldsymbol{W}_k$ follows the labeling of the quadrilateral subcell of Haj-Ali and Aboudi (2010). In this case, the bilinear term coefficients $\boldsymbol{W}_{11}$ takes the following trivial and non-trivial forms, respectively:

$$\boldsymbol{W}_{11} = \boldsymbol{0}, \quad \boldsymbol{W}_{11} = \frac{1}{2}(\boldsymbol{W}_{20} + \boldsymbol{W}_{02}) \tag{11}$$

As mentioned above, this answers the open question raised by the authors on the optimal way of handling the bilinear terms in the 2D case.

In order to establish the expressions for the strain components, the displacement gradients with respect to the physical coordinates $\boldsymbol{y}$ are needed. The standard Jacobian of the linear transformation (1) is given by:

$$J \equiv \frac{\partial(y_1, y_2, y_3)}{\partial(r, s, t)} = \begin{bmatrix} \frac{\partial y_1}{\partial r} & \frac{\partial y_2}{\partial r} & \frac{\partial y_3}{\partial r} \\ \frac{\partial y_1}{\partial s} & \frac{\partial y_2}{\partial s} & \frac{\partial y_3}{\partial s} \\ \frac{\partial y_1}{\partial t} & \frac{\partial y_2}{\partial t} & \frac{\partial y_3}{\partial t} \end{bmatrix} \tag{12}$$

Its inverse is denoted by $\hat{J} \equiv J^{-1} = \partial(r, s, t)/\partial(y_1, y_2, y_3)$ and used to relate the displacement derivatives as

$$\begin{Bmatrix} \boldsymbol{u}_{,1} \\ \boldsymbol{u}_{,2} \\ \boldsymbol{u}_{,3} \end{Bmatrix}^{(\beta)} = \left[\hat{\boldsymbol{J}}\right]^{(\beta)} \begin{Bmatrix} \boldsymbol{u}_{,r} \\ \boldsymbol{u}_{,s} \\ \boldsymbol{u}_{,t} \end{Bmatrix}^{(\beta)} \tag{13}$$

The right-hand-side can be easily established by using Eq. (3) yielding

$$\begin{aligned} \boldsymbol{u}_{,r}^{(\beta)} &= \boldsymbol{W}_{100} + \boldsymbol{W}_{110}\, s + \boldsymbol{W}_{101}\, t + 3\boldsymbol{W}_{200}\, r \\ \boldsymbol{u}_{,s}^{(\beta)} &= \boldsymbol{W}_{010} + \boldsymbol{W}_{110}\, r + \boldsymbol{W}_{011}\, t + 3\boldsymbol{W}_{020}\, s \\ \boldsymbol{u}_{,t}^{(\beta)} &= \boldsymbol{W}_{001} + \boldsymbol{W}_{101}\, r + \boldsymbol{W}_{011}\, s + 3\boldsymbol{W}_{002}\, t \end{aligned} \tag{14}$$

However, in order to express these gradients in terms of the average displacement micro-variables of the six hexahedral faces, we first define the following subcell vector with its components lumped in the following order

$$\boldsymbol{W}^{(\beta),T} = \{W_{1i}, W_{2i}, W_{3i}, W_{4i}, W_{5i}, W_{6i}, W_{0i}\}^{(\beta)} \quad i = 1, 2, 3 \tag{15}$$

Next, Eqs. (6) and (8) are used for the non-trivial case to obtain, after some manipulations, the displacement gradients with respect to the parametric variables as follows

$$\begin{Bmatrix} \boldsymbol{u}_{,r} \\ \boldsymbol{u}_{,s} \\ \boldsymbol{u}_{,t} \end{Bmatrix}^{(\beta)} = [\boldsymbol{M}]^{(\beta)} \begin{Bmatrix} \boldsymbol{W}_1 \\ \boldsymbol{W}_2 \\ \boldsymbol{W}_3 \\ \boldsymbol{W}_4 \\ \boldsymbol{W}_5 \\ \boldsymbol{W}_6 \\ \boldsymbol{W}_0 \end{Bmatrix}^{(\beta)} \tag{16}$$

where the matrix $[\mathbf{M}]^{(\beta)}$ is given by

$$\frac{1}{4}\begin{bmatrix} t & t & s & 6r+s+t+2 & s & 6r+s+t-2 & -4(3r+s+t) \\ t & t & r+6s+t-2 & r & r+6s+t+2 & r & -4(r+3s+t) \\ r+s+6t-2 & r+s+6t+2 & s & r & s & r & -4(r+s+3t) \end{bmatrix} \tag{17}$$

Similarly, Eqs. (6) and (7) provide the gradients for the trivial case as

$$\begin{Bmatrix} \boldsymbol{u}_{,r} \\ \boldsymbol{u}_{,s} \\ \boldsymbol{u}_{,t} \end{Bmatrix}^{(\beta)} = \frac{1}{2}\begin{bmatrix} 0 & 0 & 0 & 3r+1 & 0 & 3r-1 & -6r \\ 0 & 0 & 3s-1 & 0 & 3s+1 & 0 & -6s \\ 3t-1 & 3t+1 & 0 & 0 & 0 & 0 & -6t \end{bmatrix} \begin{Bmatrix} \boldsymbol{W}_1 \\ \boldsymbol{W}_2 \\ \boldsymbol{W}_3 \\ \boldsymbol{W}_4 \\ \boldsymbol{W}_5 \\ \boldsymbol{W}_6 \\ \boldsymbol{W}_0 \end{Bmatrix}^{(\beta)} \tag{18}$$

The spatial form of the strains in a given cell (β) are defined by

$$\epsilon_{ij}^{(\beta)}(\boldsymbol{y}(r,s)) = \epsilon_{ij}^{0} + \frac{1}{2}\left(\frac{\partial u_i}{\partial y_j} + \frac{\partial u_j}{\partial y_i}\right) \tag{19}$$

It is possible to bring the strains into a general matrix form

$$\boldsymbol{\epsilon}^{(\beta)} = \boldsymbol{\epsilon}^{0} + \boldsymbol{A}^{(\beta)}\boldsymbol{W}^{(\beta)} \tag{20}$$

where the strain vector notation $\boldsymbol{\epsilon}$ is defined by

$$\boldsymbol{\epsilon}^{T} = \{\epsilon_{11}, \epsilon_{22}, \epsilon_{33}, 2\epsilon_{23}, 2\epsilon_{13}, 2\epsilon_{12}\} \tag{21}$$

and $\boldsymbol{A}^{(\beta)}$ is the matrix that relates the strain to the displacement microvariables. The size of the vector $\boldsymbol{W}^{(\beta)}$ is 21 which includes all the microvariables of subcell (β) as shown in Eq. (15). Using Eqs. (17) and (18), respectively, along with Eqs. (13) and (19), it is possible to derive the strain–displacement matrix, $\boldsymbol{A}^{(\beta)}$. The non-zero components of this matrix are listed in the Appendix for the trivial and non-trivial bilinear terms.

Next, we define average traction vector $\bar{\boldsymbol{T}}^{(\beta_k)}$ on the six sides of the hexahedral subcell defined by

$$\begin{aligned} \bar{\boldsymbol{T}}^{(\beta_k)} &= \frac{1}{A_k}\int_{S_k} \boldsymbol{\sigma}^{(\beta)}(\boldsymbol{y}) \cdot \boldsymbol{n}^{(\beta_k)} dS_k \\ &= \frac{1}{4}\int_{-1}^{1}\int_{-1}^{1} \boldsymbol{\sigma}^{(\beta)}(r,s,t) \cdot \boldsymbol{n}^{(\beta_k)} d\xi_k d\eta_k, \quad k = 1,2,\ldots,6 \end{aligned} \tag{22}$$

where $\boldsymbol{n}^{(\beta_k)}$ is the unit normal vector to the kth side of subcell (β). The stress field, $\boldsymbol{\sigma}^{(\beta)}$, is given by

$$\boldsymbol{\sigma}^{(\beta)} = \boldsymbol{C}^{(\beta)} : \boldsymbol{\epsilon}^{(\beta)} \tag{23}$$

assuming a linear material behavior of the subcell, with $\boldsymbol{C}^{(\beta)}$ being the stiffness of the material in the subcell. Since the geometry is interpolated using linear mapping, the normal vector $\boldsymbol{n}^{(\beta_k)}$ to each of the six faces is constant. Employing the established spatial strains in the cell to obtain the corresponding stresses. The latter are used in the expression for the average tractions, Eq. (22). This provides

$$\begin{aligned} \bar{\boldsymbol{T}}^{(\beta_k)} &= \frac{1}{4}\int_{-1}^{1}\int_{-1}^{1} \boldsymbol{N}^{(\beta_k)}\boldsymbol{C}^{(\beta)}\left[\boldsymbol{\epsilon}^{0} + \boldsymbol{A}^{(\beta)}\boldsymbol{W}^{(\beta)}\right] d\xi_k d\eta_k \\ &= \boldsymbol{N}^{(\beta_k)}\boldsymbol{C}^{(\beta)}\left[\boldsymbol{\epsilon}^{0} + \bar{\boldsymbol{A}}^{(\beta_k)}\boldsymbol{W}^{(\beta)}\right] \end{aligned} \tag{24}$$

with,

$$\boldsymbol{N}^{(\beta_k)} = \begin{bmatrix} n_1 & 0 & 0 & 0 & n_3 & n_2 \\ 0 & n_2 & 0 & n_3 & 0 & n_1 \\ 0 & 0 & n_3 & n_2 & n_1 & 0 \end{bmatrix}^{(\beta_k)} \tag{25}$$

and

$$\bar{\boldsymbol{A}}^{(\beta_k)} = \frac{1}{4}\int_{-1}^{1}\int_{-1}^{1} \boldsymbol{A}^{(\beta)} d\xi_k d\eta_k \tag{26}$$

As mentioned above, due to the applied linear mapping, the $\boldsymbol{N}^{(\beta_k)}$ matrix is constant.

Following the original HFGMC formulation, we impose the displacements and tractions continuity between the subcells. These conditions are enforced in an average integral sense. In addition, periodicity conditions are imposed between the boundary subcells of the RUC by requiring that the displacements and tractions be continuous at these mirrored interfaces. The third major requirement of the HFGMC method is the intra subcell equilibrium applied in a volumetric average form. In the following, the above transformed expressions for the average displacements and tractions, (4) and (24), respectively can readily be used to impose the HFGMC equations. The displacements and tractions continuity can be written as

$$\bar{\boldsymbol{u}}^{(\beta_k)} = \boldsymbol{W}_k^{(\beta)} = \bar{\boldsymbol{u}}^{(\gamma_m)} = \boldsymbol{W}_m^{(\gamma)}, \quad \bar{\boldsymbol{T}}^{(\beta_k)} = \bar{\boldsymbol{T}}^{(\gamma_m)} \tag{27}$$

where (β_k) denotes the kth interface (side) of subcell (β) and (γ_m) is neighboring mth interface side of subcell (γ). The displacement and traction periodicity conditions are imposed as in Eq. (25), but with cell (β) and (γ) located on opposite sides of the RUC.

The equilibrium equations for each subcell are imposed in an average sense in conjunction with Divergence theorem in order to utilize the derived expressions for the average tractions as follows.

$$\int_V \nabla \cdot \boldsymbol{\sigma} dV = \int_S \boldsymbol{\sigma} \cdot \boldsymbol{n} dS = \sum_{k=1}^{6}\int_{S_k} \boldsymbol{N}^{(\beta_k)}\boldsymbol{\sigma}^{(\beta)} dS_k = \sum_{k=1}^{6} A_k \bar{\boldsymbol{T}}^{(\beta_k)} = \boldsymbol{0} \tag{28}$$

where V and S are the volume and surface of the (β)-subcell, respectively, and A_k is the area of the kth side.

The total number of unknown microvariables in the RUC is $21N_c$ where N_c is the total number of subcells every one of which has 21 microvariables, see Eq. (5). The number of continuity and periodicity equations for displacements is $3 \times 3N_c$ (only three interfaces for each subcell provide independent relations), see the first equality

in Eq. (27). Similarly, the number of traction continuity and periodicity equations is $3 \times 3N_c$ as shown by the second equality in Eq. (27). The average equilibrium relations, Eq. (28), provide additional $3N_c$ equations.

The above formulation completes the full theoretical derivation of the general three-dimensional parametric HFGMC micromechanical method. However, it is interesting to introduce an internal force vector $\boldsymbol{I}^{(\beta)}$ that form energy conjugate pairs with the average displacements of each side of the subcell, $\boldsymbol{W}^{(\beta)}$. The internal force vectors are directly related to the average traction defined above. These force resisting vectors are defined using external and internal work balance:

$$\boldsymbol{W}^{(\beta),T}\boldsymbol{I}^{(\beta)} \equiv \int_V \left(\boldsymbol{\epsilon}^{(\beta),T} - \boldsymbol{\epsilon}^{0,T}\right)\boldsymbol{\sigma}^{(\beta)}dV = \int_V \boldsymbol{W}^{(\beta),T}\boldsymbol{A}^{(\beta),T}\boldsymbol{\sigma}^{(\beta)}dV \tag{29}$$

and since $\boldsymbol{W}$ is arbitrary, the expression for the internal resisting vector is

$$\boldsymbol{I}^{(\beta)} = \int_V \boldsymbol{A}^{(\beta),T}\boldsymbol{\sigma}^{(\beta)}dV \tag{30}$$

The above work balance is known in the mechanics of heterogeneous media as the principal of average virtual work, e.g. Christensen (1979). For the linear material case,

$$\boldsymbol{I}^{(\beta)} = \left[\int_V \boldsymbol{A}^{(\beta),T}\boldsymbol{C}dv\right]\boldsymbol{\epsilon}^{0,(\beta)} + \left[\int_V \boldsymbol{A}^{(\beta),T}\boldsymbol{C}\boldsymbol{A}^{(\beta)}dv\right]\boldsymbol{W}^{(\beta)} \tag{31}$$

We further recognize that the first six vectors within $\boldsymbol{I}^{(\beta)}$ are the average forces, $\boldsymbol{I}^{(\beta_k)}$, on each face or side of the hexahedral subcell. The use of the above form of the average internal resisting vector, $\boldsymbol{I}^{(\beta_k)}$, instead of the average traction, $\bar{\boldsymbol{T}}^{(\beta_k)}$, in the traction continuity relation and average equilibrium, Eqs. (27) and (28), respectively, provide enhanced computational advantage mainly expressed by using the symmetric matrices in Eq. (31).

3. Implementation and computational aspects

The assembly of the derived $21 \times N_c$ HFGMC governing equations of the RUC are solved to obtain the unknown 21 microvariables for each cell. In general, equations can symbolically be grouped into three parts in the form

$$\begin{bmatrix} \mathbf{1}_u^{(+)} - \mathbf{1}_u^{(-)} \\ \mathbf{I}_T^{(+)} + \mathbf{I}_T^{(-)} \\ \sum \mathbf{I}_T \end{bmatrix} \{\mathbf{W}\} + \begin{bmatrix} \mathbf{0} \\ \mathbf{D}_T^{(+)} - \mathbf{D}_T^{(-)} \\ \sum \mathbf{D}_T \end{bmatrix} \{\boldsymbol{\epsilon}^0\} = \begin{Bmatrix} \mathbf{0} \\ \mathbf{0} \\ \mathbf{0} \end{Bmatrix} \tag{32}$$

where the first part (row) represents the average continuity and periodicity of the displacements, the second part represents the continuity of the tractions in a similar fashion. The third part represents the equilibrium equations for all the cells. The above system of equations is solved for a given externally applied strain ϵ^0 to obtain the cell microvariables. Furthermore, the local spatial strains can be readily obtained using Eq. (20), which leads to the spatial distribution of the stresses in the RUC. These can be used, for example, in a progressive analysis to determine possible damage in the constituents as well as interfacial debonding, see Haj-Ali and Aboudi (2010) for the parametric 2D-HFGMC case.

Since the first part of these equations are homogeneous and each row is composed of only two terms, expressing interface average displacement continuity becomes a straight forward manner. A pre-analysis overall RUC equivalence of matching subcells' faces can be performed similar to nodal equivalence carried out in the FE method. This can be done at the global level of the code or even using simple preprocessing subroutines. Furthermore, the equilibrium equation for each subcell, Eq. (28), expressed in either $\bar{\boldsymbol{T}}^{(\beta_k)}$ or $\boldsymbol{I}^{(\beta_k)}$, can be used in conjunction with a static condensation of the internal dependent displacement microvariables, $\boldsymbol{W}_0^{(\beta)}$. This leaves the six-side average displacements as the only set of independent variables for each subcell, which results in computational saving. The effective elastic properties of the multiphase composite can be obtained from the cell strain concentration tensors $\boldsymbol{G}^{(\beta)}$ which relates the average strain in the subcell to the externally applied strain. The latter is established by considering the average strain of the cell having the form

$$\bar{\boldsymbol{\epsilon}}^{(\beta)} = \frac{1}{V}\int_V \boldsymbol{\epsilon}(\boldsymbol{y})dV = \boldsymbol{\epsilon}^0 + \frac{1}{2V}\int_V \left(\nabla_{\boldsymbol{y}}\boldsymbol{u} + \boldsymbol{u}\nabla_{\boldsymbol{y}}\right)dV \tag{33}$$

By using the Divergence theorem and the linear mapping, Eq. (30) takes the form

$$\bar{\boldsymbol{\epsilon}}^{(\beta)} = \boldsymbol{\epsilon}^0 + \frac{1}{2V}\int_S (\boldsymbol{u}\otimes\boldsymbol{n} + \boldsymbol{n}\otimes\boldsymbol{u})dS = \boldsymbol{\epsilon}^0 + \frac{1}{2V}\sum_{k=1}^{6} A_k(\bar{\boldsymbol{u}}\otimes\boldsymbol{n} + \boldsymbol{n}\otimes\bar{\boldsymbol{u}})^{(\beta_k)} \equiv \boldsymbol{G}^{(\beta)} : \boldsymbol{\epsilon}^0 \tag{34}$$

It is observed from Eq. (34) that the concentration tensor $\boldsymbol{G}^{(\beta)}$ depends on the average displacement vectors on the surfaces of the cell. Those can be computed only after solving the entire HFGMC system of equations for the RUC as discussed above. Once the concentration tensors $\boldsymbol{G}^{(\beta)}$ have been obtained, the effective elastic stiffness tensor $\boldsymbol{C}^*$ is evaluated in the form

$$\boldsymbol{C}^* = \sum_{\beta=1}^{N_c} v_\beta \boldsymbol{C}^{(\beta)}\boldsymbol{G}^{(\beta)} \tag{35}$$

where $v_\beta = V^{(\beta)}/V_{RUC}$, and V_{RUC} being the total volume of the RUC.

It is also possible to use the intact overall system of equations, Eq. (32), without side-based condensation between the displacement microvariable. This approach allows the formulation of a new micromechanical damage approach, termed cell-extinction-damage (CED). As has been demonstrated by the 2D-HFGMC, Haj-Ali (2009) and Haj-Ali and Aboudi (2010), this cohesive micromechanical approach has the ability to perform subcell degradation along with general traction–separation between the subcells. In addition, the structure of exclusive interface-based equations unlike nodal-based FE, makes it easier to remove the subcells from the problem and/or generate average-based traction-free surfaces for crack propagation within the RUC without introducing computational instabilities.

As mentioned, linear geometric mapping and quadratic displacement interpolation (subparametric formulation) has been carried out in the previous section. This formulation has been done in order to simplify the numerical integration. Having said that, extension to full quadratic geometric mapping (isoparametric formulation) is straightforward. In both of these cases, numerical integration of the equations is needed since the Jacobian matrix is not constant. However, a computational implementation of the 2D parametric HFGMC has been reported in the literature under the name "FVDAM", e.g. Bansal and Pindera (2006). This latter 2D method assumes a volume-based constant Jacobian of the linear mapping for the geometry of the subcells. Their assumption imposes severe limitation and restriction on the parametric HFGMC method as the shape of the subcells need to be close to rectangular or parallelograms in order to maintain accurate depiction of the geometry. The use of an a priori constant Jacobian amounts to a one center-point quadrature and may lead to large solution errors especially in the displacement gradients. Furthermore, the assumption of a constant Jacobean is not applicable in the general 3D HFGMC that has full quadratic displacements. Thus, the proposed 3D parametric HFGMC has been formulated in a direct and general manner, i.e. retaining the full quadratic expansion of the displacement together with the complete Jacobian. For a more elaborate discussion on the "FVDAM" as a special case of the parametric 2D-HFGMC, see Haj-Ali and Aboudi (2012). The level of computational accuracy is determined by the number of

integration points specified within the subcell during the numerical integration of the governing equations.

It is important to draw the distinctions between the proposed parametric HFGMC and the classical displacement-based finite-element (FE) method, where a common misconception has been to link the HFGMC to FE. In the FE formulation the displacement continuity between two adjacent and connected elements is satisfied in a pointwise manner by sharing the same nodal degrees of freedom at the sides of an element. However, the HFGMC quadratic displacement expansion is nonconforming and displacement continuity is satisfied in an average sense between adjacent cells. The latter is an approximation that allows the HFGMC to explicitly use additional stress variables in the formulation and directly apply average traction continuity. The advantage of this approach is that both traction and displacement interface continuity between different materials can be directly employed. Further, cohesive damage modeling can be easily employed as mentioned before for the 2D case. Unlike FE, the HFGMC is a specialized micromechanical modeling framework in which the remote fields are directly tied to the micromechanical formulation (e.g. the remote average strain is directly used in the HFGMC formulation). On the other hand, the periodicity in the FE formulation is imposed only through displacement boundary conditions, while in the HFGMC, the periodic boundary conditions are imposed directly using both the average displacement and tractions. The latter differences are illustrated in the next application section where examples for RUCs with both traction and displacement periodic conditions are compared to FE RUCs modeled with applied far-field nodal displacements. Having said that, it is possible to draw an analogy between the FE (standard or hybrid forms) and the HFGMC method by considering the average displacement microvariables as face or side-based generalized displacements variables. This analogy allows the use of the average virtual work principal to define the internal force vector and its associate symmetric matrices which are useful for the solution of the overall system of equations. Therefore, the HFGMC is a micromechanical method of analysis that should be viewed as a stand-alone method of solution on its own right. It has been shown that it offers a specialized combined local and global solution fields suitable for the analysis of periodic composites. The present HFGMC-3D subcell has 21 independent quadratic coefficient variables with linear geometric parametric mapping. As for computational efficiency, it will be difficult to directly compare the HFGMC with an isoparametric FE element. Having said that, the offered HFGMC parametric quadratic formulation provides an additional computational efficiency as compared to the 24 variables that belong to a linear-based 3D finite element.

4. Applications

Several applications are performed to show the effectiveness of the parametric HFGMC method in capturing the spatial stress field distributions within the phases of triply periodic composites. To this end, RUCs are generated with coarse and refined resolutions using hexahedral subcells. Selected stress fields are compared with solutions of RUCs using displacement based FE models. In order to compare the parametric HFGMC and the FE solutions, the full periodic conditions between the boundary surfaces of the RUC, i.e. both traction and displacement continuity on mirrored boundary surfaces, were not applied. It is important to mention that the full periodic conditions are an integral part of the HFGMC formulation, however, full periodicity is not a straightforward using the displacement-based FE. Thus, the boundary conditions imposed in all compared cases, unless stated otherwise, are:

$$\boldsymbol{u}^0(S) = \boldsymbol{\epsilon}^0 \cdot \mathbf{x} \tag{36}$$

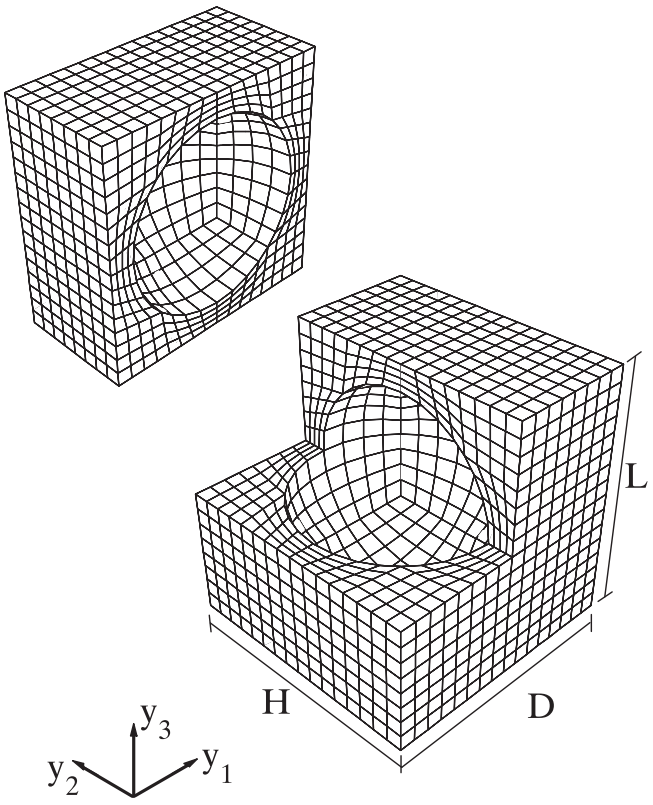

Fig. 3. Parametric HFGMC meshes for an RUC with spherical cavity.

where (S) here is the outside periodic surface of the RUC, $\boldsymbol{\epsilon}^0$ is the applied average strain and $\mathbf{x}$ are the coordinates of the surface points. In the case of the FE-RUC, constrains were written for the boundary nodes that link their degrees of freedom to the applied average strain. However, for the case of the RUC modeled with the HFGMC, the average displacement microvariables on the

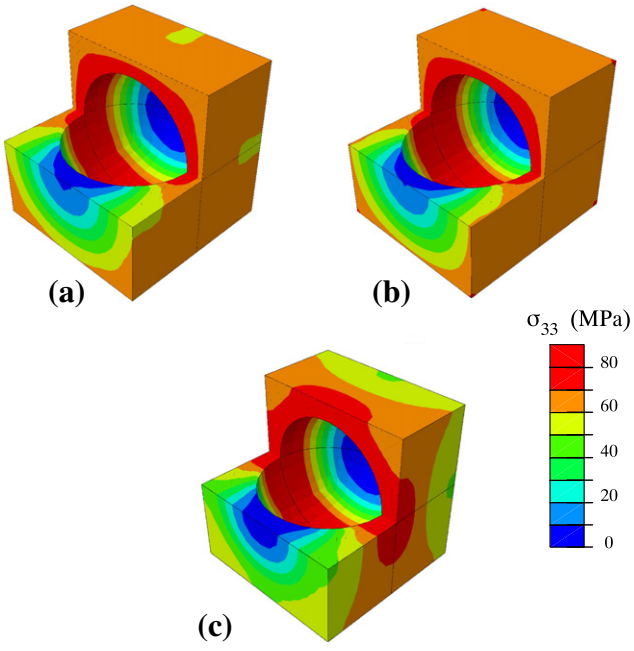

Fig. 4. Stress distributions in the RUC with a spherical cavity. (a) HFGMC results (periodic displacements), (b) FE results (periodic displacements), and (c) HFGMC results (periodic displacements and tractions).

subcells with boundary faces were set to zero. Select cases for HFGMC-RUCs with full periodic boundary conditions are presented in order to show the different spatial distribution of the local fields that the can be achieved using the HFGMC.

The first RUC model is for a medium with repeated spherical cavities, thus forming a porous material. Fig. 3 shows the geometry of this problem in the form of a half RUC cut at the mid-plane and another with a quarter portion removed. It should be mentioned that while it is possible to apply symmetric conditions, the full geometry is simulated. The dimensions of the RUC were taken as $D = H = L = 1$ and the radius of the spherical cavity was $R = 0.4$. The material Young's modulus and Poisson's ratio elastic properties are $E = 4.8$ GPa, $\nu = 0.34$. The composite is subjected to a remote uniaxial strain loading of $\epsilon^0_{11} = 0.01$. The number of hexahedral subcells used to map the geometry was $N_c = 3584$. This discretization of the RUC is not considered as a refined one compared to the number of subcells needed to capture the local spherical shape curvature. This was the choice in order to demonstrate the ability of the HFGMC to accurately solve for the local fields despite the use of average traction and displacements. Fig. 4(a) and (b) show the σ_{11} stress distributions for the HFGMC and the FE models, respectively. In these two cases, only the displacement-based periodic conditions were enforced. It is clear that the stress distribution from the HFGMC solution is quite identical to the one obtained from the FE model despite the use of relatively smaller number of independent solution variables. As mentioned, each subcell has $21N_c$ total independent average displacement microvariables in the case of the HFGMC among of which many dependent displacements are condensed due to subcells inter-continuity at the global system of equations as discussed in the implementations section. Therefore, the element that was selected for the FE RUC cases is the 8-nodes linear brick which has $8 \times 3 \times N_c = 24N_c$ number of variables having both RUCs close in their problem size. Fig. 4(c) shows the stress distribution generated by the HFGMC, however, the full periodic conditions were applied in this case. It is evident that the local spatial distribution is affected at the boundaries of the RUCs if accurate periodicity needs to be captured. In the case where the effective elastic properties of the entire medium are sought, applying full or partial periodic conditions may not yield pronounced differences. Our aim in the parametric HFGMC is to provide an analysis tool capable of accurately predicting the local fields.

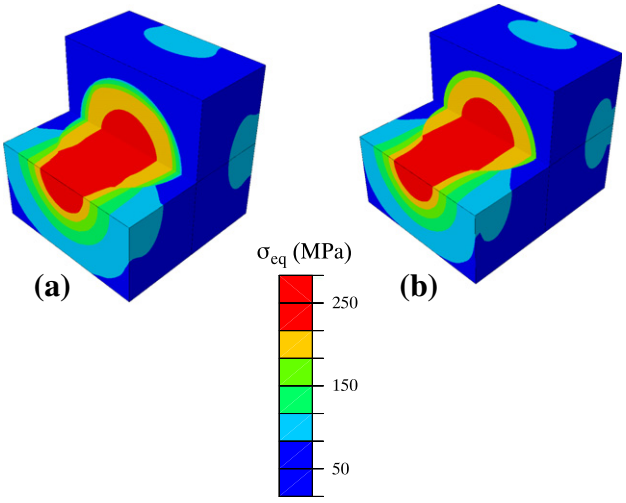

Fig. 6. Stress distributions in the RUC with a spherical inclusion. (a) HFGMC results, (b) FE results.

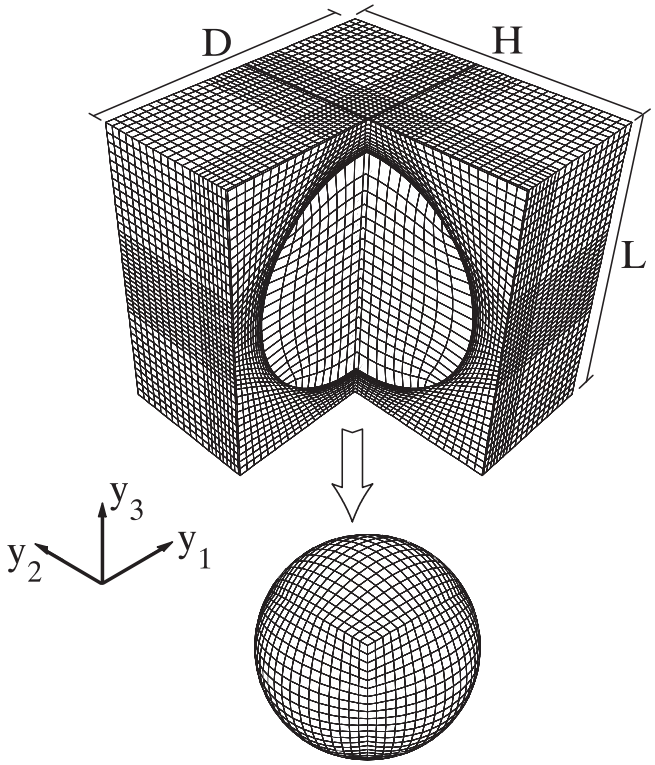

Fig. 5. Parametric HFGMC 3D meshes for an RUC with spherical inclusion using hexahedral subcells.

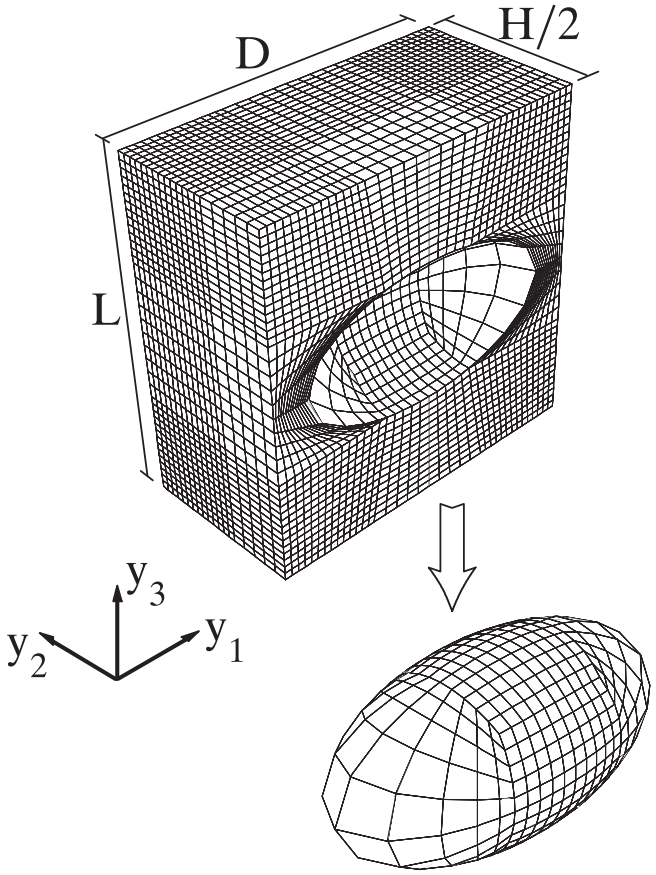

Fig. 7. Parametric HFGMC 3D meshes for an RUC with spheroidal inclusion using hexahedral subcells.

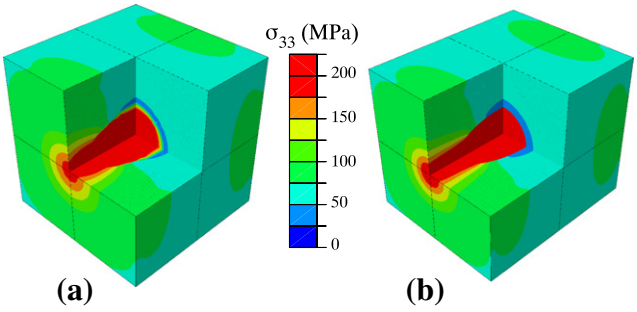

Fig. 8. Stress distributions in the RUC with a spheroidal inclusion. (a) HFGMC results, (b) FE results.

The next application deals with a composite with spherical inclusions, thus forming a particulate composite. Fig. 5 shows the discretized RUC with $D = H = L = 1$ and the radius of the spherical inclusion is $R = 0.4$, which corresponds to inclusion volume fraction of 26.8%. An effort has been made to use a refined mesh at the interface of the spherical inclusion. The elastic properties of the inclusion and the matrix are: $E = 380$ GPa, $v = 0.1$ and $E = 4.8$ GPa, $v = 0.34$, respectively. The far field applied strain is $\epsilon^0_{33} = 0.01$. The number of hexahedral subcells used for both HFGMC and FE is $N_c = 74088$. Fig. 6(a) and (b) show the Mises stress distributions as predicted by the HFGMC and the FE, respectively, in the direction of the applied strain. Here, excellent agreement between the two solutions is exhibited. As a continuation of this problem, we consider an ellipsoidal inclusion, the mesh of which is shown in Fig. 7. It illustrates a half RUC with removed inclusion and the ellipsoidal inclusion. A coarser mesh is used for the latter in order to minimize the size of the problem: $N_c = 54872$. The dimensions of the RUC are $D = H = L = 1$ and the major and two minor axes of the ellipsoid are $0.8, 0.4$ and 0.4 (spheroidal shape), respectively. The same elastic properties for the inclusion and matrix as well as the magnitude of the applied far field are chosen as in the previous problem. Fig. 8 displays the resulting stress σ_{33} distribution in the major-axis direction of

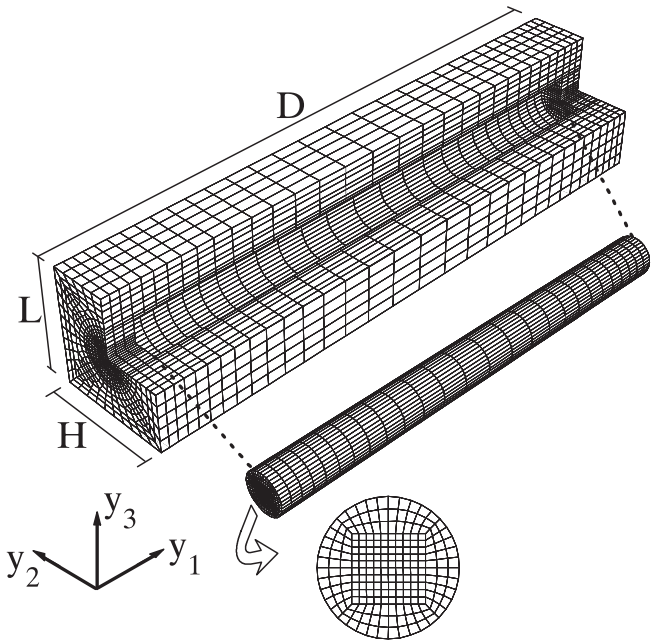

Fig. 9. Parametric HFGMC 3D meshes for an RUC, with discontinuous aligned fiber having a circular cross-section, using hexahedral subcells.

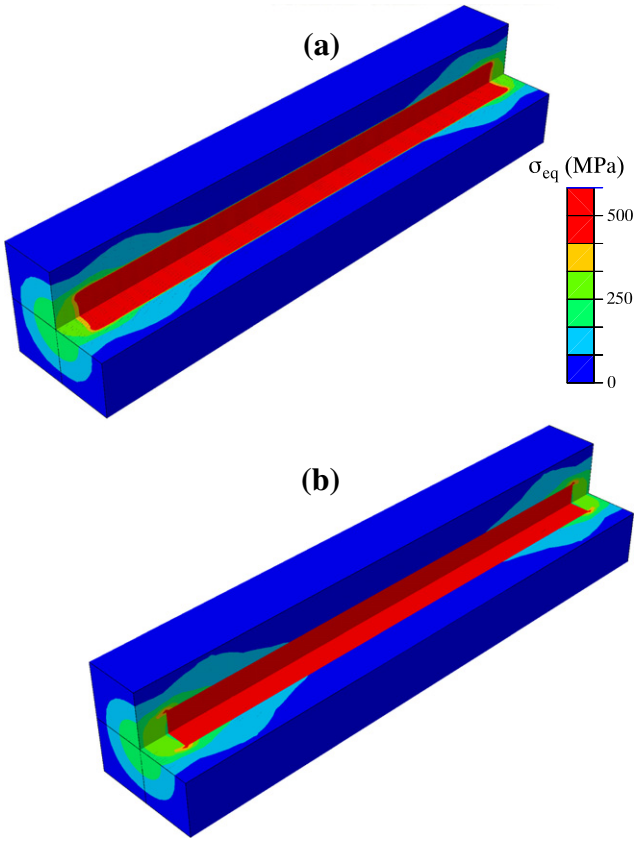

Fig. 10. Stress distributions in the RUC with the discontinuous fiber. (a) HFGMC results, (b) FE results.

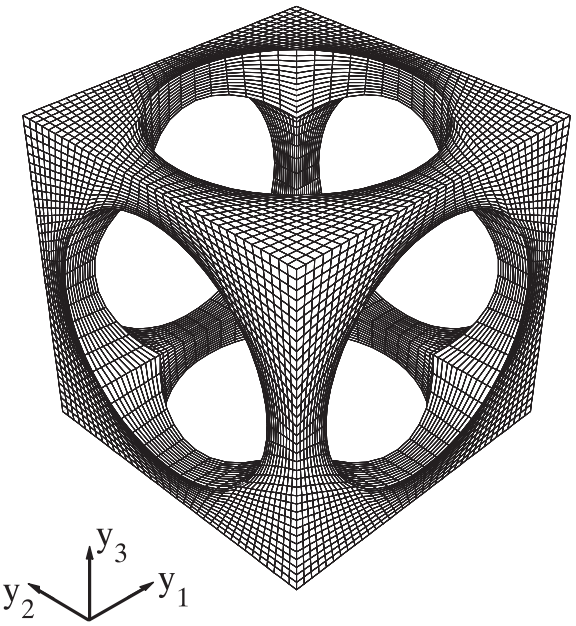

Fig. 11. Parametric HFGMC mesh for an RUC of a foam material.

the ellipsoid for both the HFGMC and FE solutions and for the full RUC with quarter portion removed. Again, a very good agreement exists.

The next studied problem analyzes a composite with a system of reinforcements in the form of discontinuous aligned circular fibers (short-fiber composite). Fig. 9 displays the refined mesh of the

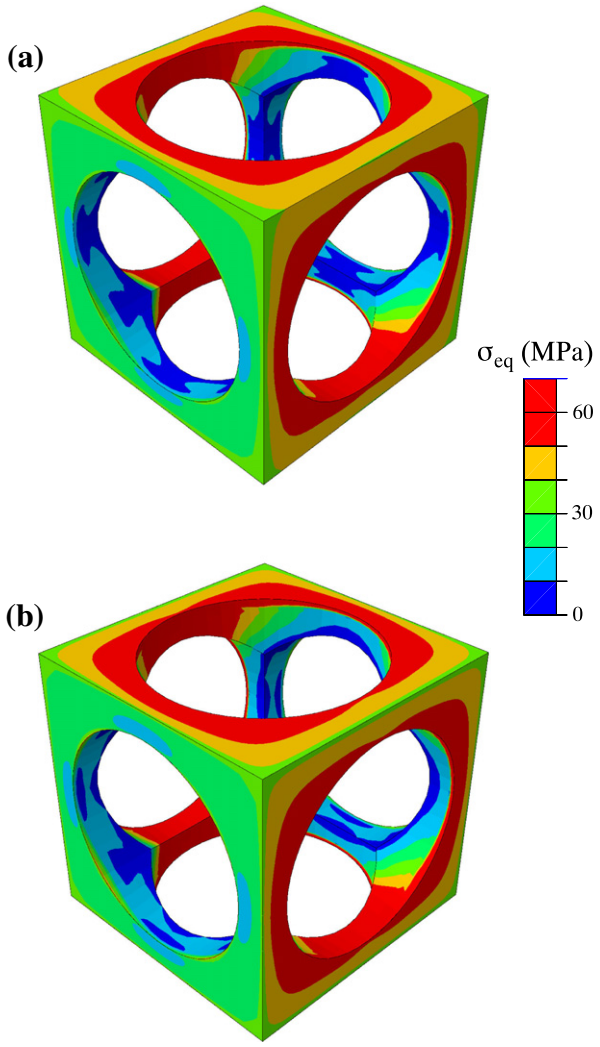

Fig. 12. Stress distributions in the RUC of the foam material. (a) HFGMC results (periodic displacements), (b) FE results (periodic displacements).

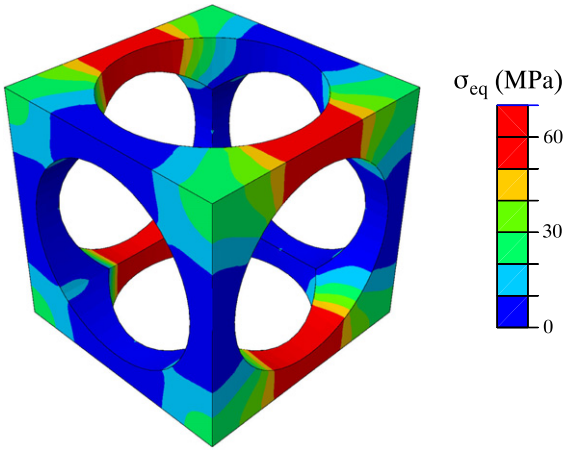

Fig. 13. Stress distributions in the RUC of the foam material showing HFGMC results with full periodic conditions (displacements and tractions).

RUC together with the short fiber itself and its cross-section. The ratios of the dimensions of the RUC are $D = 5$ and $H = L = 1$. The axial length of the fiber is 4.53 and its diameter is equal to 0.4, resulting in a fiber volume fraction of 11.4%. The RUC is subjected to remote axial strain $\epsilon^0_{11} = 0.01$. The values of the fiber and matrix elastic properties are the same as those of the inclusion and matrix properties in the previous problem. The size of the problem in this case is $N_c = 17984$. The resulting Mises stress distribution within the RUC as predicted by the HFGMC and the FE are shown in Fig. 10(a) and (b), respectively. It can be observed that the HFGMC is capable in capturing the local mechanism of stress-transfer at the discontinuous edge of the fiber to the matrix. Both solutions are very close as shown.

The final example considers a periodic foam-like material with a relatively complex geometry of the microstructure. Fig. 11 shows the selected geometry of the RUC. It is evident that this is a relatively complex geometry due to the spatial curvature and shape of the cuts. Accurate modeling of the material in this case requires a refined 3D mesh able to represent the local geometry. The choice of the RUC geometry has been inspired from scaffolds used in tissue engineering and orthopedic micro-implants. Its dimensions are $D = H = L = 1$ and was constructed by removing material enclosed by three orthogonal cylinders, the diameter of each is 0.8. It is worth observing the local geometry where the removed cylinders intersect. The material elastic properties are $E = 4.8$ GPa, $\nu = 0.34$. The total number of subcells is $N_c = 34560$ and the remote axial strain is $\epsilon^0_{11} = 0.01$. Fig. 12(a) and (b) exhibit the Mises stress distribution in the 3D HFGMC compared with the FE solution, respectively. Excellent agreement exists especially at the inner corners. It is important to mention for this case, that an explicit average traction-free conditions are imposed by the HFGMC on the inner surfaces. Finally, the Mises stress variations are shown in Fig. 13 for the same RUC but when full periodicity conditions are applied between the RUCs by the HFGMC model. It is clearly observed that the form of the stress distribution is impacted by imposing the full micromechanical boundary conditions. This demonstrates the micromechanical capability embedded in the formulation of the HFGMC. By introducing inelastic effects, it would be possible to extend the 3D parametric HFGMC to analyze metallic foams.

5. Conclusions

A new 3D parametric micromechanical formulation of the HFGMC method is presented using linear geometric mapping with hexahedral subcells. A complete quadratic expansion of the displacement is used for the subcells where its unknown coefficients are in the form of average displacements of the six sides of the subcells in addition to an internal coefficient that can be statically condensed using the integral-based equilibrium equations. The independent average displacement micro-variable vector for each side of the subcell forms an energy-conjugate pair with the transformed average-traction vector. Trivial and non-trivial relations for the coefficients of the bilinear terms are found and their corresponding strain–displacement matrices are derived without the need for additional equations in the form of moments of the equilibrium. Thus, the open question previously posed by the authors on the optimal equations for the bilinear coefficients is resolved in the current study. The previous 2D parametric and orthogonal HFGMC formulations are special cases of the present 3D formulation. Solution approaches to the parametric HFGMC equations are also discussed and numerical integration is needed due to non constant Jacobian of the linear mapping. Wide range of applications are presented to verify the 3D parametric HFGMC as compared with finite-element RUC models. The proposed 3D parametric HFGMC is general and well suited for nonlinear material and finite-deformations previously developed in the framework of the orthogonal HFGMC. Previously developed cohesive damage modeling can be integrated within the new formulation. These modeling

features can be integrated within the proposed 3D parametric micromechanics along with local–global multi-scale analysis of composite structures.

Acknowledgments

The partial support from the European-Union Marie-Curie IRG and the German–Israel Foundation (GIF) Grants are gratefully acknowledged.

Appendix A

In this Appendix, the non-zero components of the strain micro-displacements matrices are listed first for the quadratic polynomial with zero bilinear terms (trivial case) and second for the constrained symmetric bilinear term coefficients (non-trivial case). The terms for first matrix are

$$A_{1,1}=-1/2\hat{J}_{1,3}+3/2\hat{J}_{1,3}t \quad A_{1,4}=1/2\hat{J}_{1,3}+3/2\hat{J}_{1,3}t$$

$$A_{1,7}=-1/2\hat{J}_{1,2}+3/2\hat{J}_{1,2}s \quad A_{1,10}=1/2\hat{J}_{1,1}+3/2\hat{J}_{1,1}r$$

$$A_{1,13}=1/2\hat{J}_{1,2}+3/2\hat{J}_{1,2}s \quad A_{1,16}=-1/2\hat{J}_{1,1}+3/2\hat{J}_{1,1}r$$

$$A_{1,19}=-3\hat{J}_{1,1}r-3\hat{J}_{1,2}s-3\hat{J}_{1,3}t \quad A_{2,2}=-1/2\hat{J}_{2,3}+3/2\hat{J}_{2,3}t$$

$$A_{2,5}=1/2\hat{J}_{2,3}+3/2\hat{J}_{2,3}t \quad A_{2,8}=-1/2\hat{J}_{2,2}+3/2\hat{J}_{2,2}s$$

$$A_{2,11}=1/2\hat{J}_{2,1}+3/2\hat{J}_{2,1}r \quad A_{2,14}=1/2\hat{J}_{2,2}+3/2\hat{J}_{2,2}s$$

$$A_{2,17}=-1/2\hat{J}_{2,1}+3/2\hat{J}_{2,1}r \quad A_{2,20}=-3\hat{J}_{2,1}r-3\hat{J}_{2,2}s-3\hat{J}_{2,3}t$$

$$A_{3,3}=-1/2\hat{J}_{3,3}+3/2\hat{J}_{3,3}t \quad A_{3,6}=1/2\hat{J}_{3,3}+3/2\hat{J}_{3,3}t$$

$$A_{3,9}=-1/2\hat{J}_{3,2}+3/2\hat{J}_{3,2}s \quad A_{3,12}=1/2\hat{J}_{3,1}+3/2\hat{J}_{3,1}r$$

$$A_{3,15}=1/2\hat{J}_{3,2}+3/2\hat{J}_{3,2}s \quad A_{3,18}=-1/2\hat{J}_{3,1}+3/2\hat{J}_{3,1}r$$

$$A_{3,21}=-3\hat{J}_{3,1}r-3\hat{J}_{3,2}s-3\hat{J}_{3,3}t \quad A_{4,2}=-1/2\hat{J}_{3,3}+3/2\hat{J}_{3,3}t$$

$$A_{4,3}=-1/2\hat{J}_{2,3}+3/2\hat{J}_{2,3}t \quad A_{4,5}=1/2\hat{J}_{3,3}+3/2\hat{J}_{3,3}t$$

$$A_{4,6}=1/2\hat{J}_{2,3}+3/2\hat{J}_{2,3}t \quad A_{4,8}=-1/2\hat{J}_{3,2}+3/2\hat{J}_{3,2}s$$

$$A_{4,9}=-1/2\hat{J}_{2,2}+3/2\hat{J}_{2,2}s \quad A_{4,11}=1/2\hat{J}_{3,1}+3/2\hat{J}_{3,1}r$$

$$A_{4,12}=1/2\hat{J}_{2,1}+3/2\hat{J}_{2,1}r \quad A_{4,14}=1/2\hat{J}_{3,2}+3/2\hat{J}_{3,2}s$$

$$A_{4,15}=1/2\hat{J}_{2,2}+3/2\hat{J}_{2,2}s \quad A_{4,17}=-1/2\hat{J}_{3,1}+3/2\hat{J}_{3,1}r$$

$$A_{4,18}=-1/2\hat{J}_{2,1}+3/2\hat{J}_{2,1}r \quad A_{4,20}=-3\hat{J}_{3,1}r-3\hat{J}_{3,2}s-3\hat{J}_{3,3}t$$

$$A_{4,21}=-3\hat{J}_{2,1}r-3\hat{J}_{2,2}s-3\hat{J}_{2,3}t \quad A_{5,1}=-1/2\hat{J}_{3,3}+3/2\hat{J}_{3,3}t$$

$$A_{5,3}=-1/2\hat{J}_{1,3}+3/2\hat{J}_{1,3}t \quad A_{5,4}=1/2\hat{J}_{3,3}+3/2\hat{J}_{3,3}t$$

$$A_{5,6}=1/2\hat{J}_{1,3}+3/2\hat{J}_{1,3}t \quad A_{5,7}=-1/2\hat{J}_{3,2}+3/2\hat{J}_{3,2}s$$

$$A_{5,9}=-1/2\hat{J}_{1,2}+3/2\hat{J}_{1,2}s \quad A_{5,10}=1/2\hat{J}_{3,1}+3/2\hat{J}_{3,1}r$$

$$A_{5,12}=1/2\hat{J}_{1,1}+3/2\hat{J}_{1,1}r \quad A_{5,13}=1/2\hat{J}_{3,2}+3/2\hat{J}_{3,2}s$$

$$A_{5,15}=1/2\hat{J}_{1,2}+3/2\hat{J}_{1,2}s \quad A_{5,16}=-1/2\hat{J}_{3,1}+3/2\hat{J}_{3,1}r$$

$$A_{5,18}=-1/2\hat{J}_{1,1}+3/2\hat{J}_{1,1}r \quad A_{5,19}=-3\hat{J}_{3,1}r-3\hat{J}_{3,2}s-3\hat{J}_{3,3}t$$

$$A_{5,21}=-3\hat{J}_{1,1}r-3\hat{J}_{1,2}s-3\hat{J}_{1,3}t \quad A_{6,1}=-1/2\hat{J}_{2,3}+3/2\hat{J}_{2,3}t$$

$$A_{6,2}=-1/2\hat{J}_{1,3}+3/2\hat{J}_{1,3}t \quad A_{6,4}=1/2\hat{J}_{2,3}+3/2\hat{J}_{2,3}t$$

$$A_{6,5}=1/2\hat{J}_{1,3}+3/2\hat{J}_{1,3}t \quad A_{6,7}=-1/2\hat{J}_{2,2}+3/2\hat{J}_{2,2}s$$

$$A_{6,8}=-1/2\hat{J}_{1,2}+3/2\hat{J}_{1,2}s \quad A_{6,10}=1/2\hat{J}_{2,1}+3/2\hat{J}_{2,1}r$$

$$A_{6,11}=1/2\hat{J}_{1,1}+3/2\hat{J}_{1,1}r \quad A_{6,13}=1/2\hat{J}_{2,2}+3/2\hat{J}_{2,2}s$$

$$A_{6,14}=1/2\hat{J}_{1,2}+3/2\hat{J}_{1,2}s \quad A_{6,16}=-1/2\hat{J}_{2,1}+3/2\hat{J}_{2,1}r$$

$$A_{6,17}=-1/2\hat{J}_{1,1}+3/2\hat{J}_{1,1}r \quad A_{6,19}=-3\hat{J}_{2,1}r-3\hat{J}_{2,2}s-3\hat{J}_{2,3}t$$

$$A_{6,20}=-3\hat{J}_{1,1}r-3\hat{J}_{1,2}s-3\hat{J}_{1,3}t$$

The non-zero terms for the second matrix are

$$A_{1,1}=1/4\hat{J}_{1,3}r+1/4\hat{J}_{1,3}s+\left(1/4\hat{J}_{1,1}+1/4\hat{J}_{1,2}+3/2\hat{J}_{1,3}\right)t-1/2\hat{J}_{1,3}$$

$$A_{1,4}=1/4\hat{J}_{1,3}r+1/4\hat{J}_{1,3}s+\left(1/4\hat{J}_{1,1}+1/4\hat{J}_{1,2}+3/2\hat{J}_{1,3}\right)t+1/2\hat{J}_{1,3}$$

$$A_{1,7}=1/4\hat{J}_{1,2}r+\left(1/4\hat{J}_{1,1}+3/2\hat{J}_{1,2}+1/4\hat{J}_{1,3}\right)s-1/2\hat{J}_{1,2}+1/4\hat{J}_{1,2}t$$

$$A_{1,10}=\left(3/2\hat{J}_{1,1}+1/4\hat{J}_{1,2}+1/4\hat{J}_{1,3}\right)r+1/2\hat{J}_{1,1}+1/4\hat{J}_{1,1}s+1/4\hat{J}_{1,1}t$$

$$A_{1,13}=1/4\hat{J}_{1,2}r+\left(1/4\hat{J}_{1,1}+3/2\hat{J}_{1,2}+1/4\hat{J}_{1,3}\right)s+1/2\hat{J}_{1,2}+1/4\hat{J}_{1,2}t$$

$$A_{1,16}=\left(3/2\hat{J}_{1,1}+1/4\hat{J}_{1,2}+1/4\hat{J}_{1,3}\right)r-1/2\hat{J}_{1,1}+1/4\hat{J}_{1,1}s+1/4\hat{J}_{1,1}t$$

$$A_{1,19}=\left(-\hat{J}_{1,3}-\hat{J}_{1,2}-3\hat{J}_{1,1}\right)r+\left(-\hat{J}_{1,3}-3\hat{J}_{1,2}-\hat{J}_{1,1}\right)s+\left(-3\hat{J}_{1,3}-\hat{J}_{1,2}-\hat{J}_{1,1}\right)t$$

$$A_{2,2}=1/4\hat{J}_{2,3}r+1/4\hat{J}_{2,3}s+\left(1/4\hat{J}_{2,1}+1/4\hat{J}_{2,2}+3/2\hat{J}_{2,3}\right)t-1/2\hat{J}_{2,3}$$

$$A_{2,5}=1/4\hat{J}_{2,3}r+1/4\hat{J}_{2,3}s+\left(1/4\hat{J}_{2,1}+1/4\hat{J}_{2,2}+3/2\hat{J}_{2,3}\right)t+1/2\hat{J}_{2,3}$$

$$A_{2,8}=1/4\hat{J}_{2,2}r+\left(1/4\hat{J}_{2,1}+3/2\hat{J}_{2,2}+1/4\hat{J}_{2,3}\right)s-1/2\hat{J}_{2,2}+1/4\hat{J}_{2,2}t$$

$$A_{2,11}=\left(3/2\hat{J}_{2,1}+1/4\hat{J}_{2,2}+1/4\hat{J}_{2,3}\right)r+1/2\hat{J}_{2,1}+1/4\hat{J}_{2,1}s+1/4\hat{J}_{2,1}t$$

$$A_{2,14}=1/4\hat{J}_{2,2}r+\left(1/4\hat{J}_{2,1}+3/2\hat{J}_{2,2}+1/4\hat{J}_{2,3}\right)s+1/2\hat{J}_{2,2}+1/4\hat{J}_{2,2}t$$

$$A_{2,17}=\left(3/2\hat{J}_{2,1}+1/4\hat{J}_{2,2}+1/4\hat{J}_{2,3}\right)r-1/2\hat{J}_{2,1}+1/4\hat{J}_{2,1}s+1/4\hat{J}_{2,1}t$$

$$A_{2,20}=\left(-\hat{J}_{2,3}-\hat{J}_{2,2}-3\hat{J}_{2,1}\right)r+\left(-\hat{J}_{2,3}-3\hat{J}_{2,2}-\hat{J}_{2,1}\right)s+\left(-3\hat{J}_{2,3}-\hat{J}_{2,2}-\hat{J}_{2,1}\right)t$$

$$A_{3,3} = 1/4\hat{J}_{3,3}r + 1/4\hat{J}_{3,3}s + \left(1/4\hat{J}_{3,1} + 1/4\hat{J}_{3,2} + 3/2\hat{J}_{3,3}\right)t - 1/2\hat{J}_{3,3}$$

$$A_{3,6} = 1/4\hat{J}_{3,3}r + 1/4\hat{J}_{3,3}s + \left(1/4\hat{J}_{3,1} + 1/4\hat{J}_{3,2} + 3/2\hat{J}_{3,3}\right)t + 1/2\hat{J}_{3,3}$$

$$A_{3,9} = 1/4\hat{J}_{3,2}r + \left(1/4\hat{J}_{3,1} + 3/2\hat{J}_{3,2} + 1/4\hat{J}_{3,3}\right)s - 1/2\hat{J}_{3,2} + 1/4\hat{J}_{3,2}t$$

$$A_{3,12} = \left(3/2\hat{J}_{3,1} + 1/4\hat{J}_{3,2} + 1/4\hat{J}_{3,3}\right)r + 1/2\hat{J}_{3,1} + 1/4\hat{J}_{3,1}s + 1/4\hat{J}_{3,1}t$$

$$A_{3,15} = 1/4\hat{J}_{3,2}r + \left(1/4\hat{J}_{3,1} + 3/2\hat{J}_{3,2} + 1/4\hat{J}_{3,3}\right)s + 1/2\hat{J}_{3,2} + 1/4\hat{J}_{3,2}t$$

$$A_{3,18} = \left(3/2\hat{J}_{3,1} + 1/4\hat{J}_{3,2} + 1/4\hat{J}_{3,3}\right)r - 1/2\hat{J}_{3,1} + 1/4\hat{J}_{3,1}s + 1/4\hat{J}_{3,1}t$$

$$A_{3,21} = \left(-\hat{J}_{3,3} - \hat{J}_{3,2} - 3\hat{J}_{3,1}\right)r + \left(-\hat{J}_{3,3} - 3\hat{J}_{3,2} - \hat{J}_{3,1}\right) s + \left(-3\hat{J}_{3,3} - \hat{J}_{3,2} - \hat{J}_{3,1}\right)t$$

$$A_{4,2} = 1/4\hat{J}_{3,3}r + 1/4\hat{J}_{3,3}s + \left(1/4\hat{J}_{3,1} + 1/4\hat{J}_{3,2} + 3/2\hat{J}_{3,3}\right)t - 1/2\hat{J}_{3,3}$$

$$A_{4,3} = 1/4\hat{J}_{2,3}r + 1/4\hat{J}_{2,3}s + \left(1/4\hat{J}_{2,1} + 1/4\hat{J}_{2,2} + 3/2\hat{J}_{2,3}\right)t - 1/2\hat{J}_{2,3}$$

$$A_{4,5} = 1/4\hat{J}_{3,3}r + 1/4\hat{J}_{3,3}s + \left(1/4\hat{J}_{3,1} + 1/4\hat{J}_{3,2} + 3/2\hat{J}_{3,3}\right)t + 1/2\hat{J}_{3,3}$$

$$A_{4,6} = 1/4\hat{J}_{2,3}r + 1/4\hat{J}_{2,3}s + \left(1/4\hat{J}_{2,1} + 1/4\hat{J}_{2,2} + 3/2\hat{J}_{2,3}\right)t + 1/2\hat{J}_{2,3}$$

$$A_{4,8} = 1/4\hat{J}_{3,2}r + \left(1/4\hat{J}_{3,1} + 3/2\hat{J}_{3,2} + 1/4\hat{J}_{3,3}\right)s - 1/2\hat{J}_{3,2} + 1/4\hat{J}_{3,2}t$$

$$A_{4,9} = 1/4\hat{J}_{2,2}r + \left(1/4\hat{J}_{2,1} + 3/2\hat{J}_{2,2} + 1/4\hat{J}_{2,3}\right)s - 1/2\hat{J}_{2,2} + 1/4\hat{J}_{2,2}t$$

$$A_{4,11} = \left(3/2\hat{J}_{3,1} + 1/4\hat{J}_{3,2} + 1/4\hat{J}_{3,3}\right)r + 1/2\hat{J}_{3,1} + 1/4\hat{J}_{3,1}s + 1/4\hat{J}_{3,1}t$$

$$A_{4,12} = \left(3/2\hat{J}_{2,1} + 1/4\hat{J}_{2,2} + 1/4\hat{J}_{2,3}\right)r + 1/2\hat{J}_{2,1} + 1/4\hat{J}_{2,1}s + 1/4\hat{J}_{2,1}t$$

$$A_{4,14} = 1/4\hat{J}_{3,2}r + \left(1/4\hat{J}_{3,1} + 3/2\hat{J}_{3,2} + 1/4\hat{J}_{3,3}\right)s + 1/2\hat{J}_{3,2} + 1/4\hat{J}_{3,2}t$$

$$A_{4,15} = 1/4\hat{J}_{2,2}r + \left(1/4\hat{J}_{2,1} + 3/2\hat{J}_{2,2} + 1/4\hat{J}_{2,3}\right)s + 1/2\hat{J}_{2,2} + 1/4\hat{J}_{2,2}t$$

$$A_{4,17} = \left(3/2\hat{J}_{3,1} + 1/4\hat{J}_{3,2} + 1/4\hat{J}_{3,3}\right)r - 1/2\hat{J}_{3,1} + 1/4\hat{J}_{3,1}s + 1/4\hat{J}_{3,1}t$$

$$A_{4,18} = \left(3/2\hat{J}_{2,1} + 1/4\hat{J}_{2,2} + 1/4\hat{J}_{2,3}\right)r - 1/2\hat{J}_{2,1} + 1/4\hat{J}_{2,1}s + 1/4\hat{J}_{2,1}t$$

$$A_{4,20} = \left(-\hat{J}_{3,3} - \hat{J}_{3,2} - 3\hat{J}_{3,1}\right)r + \left(-\hat{J}_{3,3} - 3\hat{J}_{3,2} - \hat{J}_{3,1}\right) s + \left(-3\hat{J}_{3,3} - \hat{J}_{3,2} - \hat{J}_{3,1}\right)t$$

$$A_{4,21} = \left(-\hat{J}_{2,3} - \hat{J}_{2,2} - 3\hat{J}_{2,1}\right)r + \left(-\hat{J}_{2,3} - 3\hat{J}_{2,2} - \hat{J}_{2,1}\right) s + \left(-3\hat{J}_{2,3} - \hat{J}_{2,2} - \hat{J}_{2,1}\right)t$$

$$A_{5,1} = 1/4\hat{J}_{3,3}r + 1/4\hat{J}_{3,3}s + \left(1/4\hat{J}_{3,1} + 1/4\hat{J}_{3,2} + 3/2\hat{J}_{3,3}\right)t - 1/2\hat{J}_{3,3}$$

$$A_{5,3} = 1/4\hat{J}_{1,3}r + 1/4\hat{J}_{1,3}s + \left(1/4\hat{J}_{1,1} + 1/4\hat{J}_{1,2} + 3/2\hat{J}_{1,3}\right)t - 1/2\hat{J}_{1,3}$$

$$A_{5,4} = 1/4\hat{J}_{3,3}r + 1/4\hat{J}_{3,3}s + \left(1/4\hat{J}_{3,1} + 1/4\hat{J}_{3,2} + 3/2\hat{J}_{3,3}\right)t + 1/2\hat{J}_{3,3}$$

$$A_{5,6} = 1/4\hat{J}_{1,3}r + 1/4\hat{J}_{1,3}s + \left(1/4\hat{J}_{1,1} + 1/4\hat{J}_{1,2} + 3/2\hat{J}_{1,3}\right)t + 1/2\hat{J}_{1,3}$$

$$A_{5,7} = 1/4\hat{J}_{3,2}r + \left(1/4\hat{J}_{3,1} + 3/2\hat{J}_{3,2} + 1/4\hat{J}_{3,3}\right)s - 1/2\hat{J}_{3,2} + 1/4\hat{J}_{3,2}t$$

$$A_{5,9} = 1/4\hat{J}_{1,2}r + \left(1/4\hat{J}_{1,1} + 3/2\hat{J}_{1,2} + 1/4\hat{J}_{1,3}\right)s - 1/2\hat{J}_{1,2} + 1/4\hat{J}_{1,2}t$$

$$A_{5,10} = \left(3/2\hat{J}_{3,1} + 1/4\hat{J}_{3,2} + 1/4\hat{J}_{3,3}\right)r + 1/2\hat{J}_{3,1} + 1/4\hat{J}_{3,1}s + 1/4\hat{J}_{3,1}t$$

$$A_{5,12} = \left(3/2\hat{J}_{1,1} + 1/4\hat{J}_{1,2} + 1/4\hat{J}_{1,3}\right)r + 1/2\hat{J}_{1,1} + 1/4\hat{J}_{1,1}s + 1/4\hat{J}_{1,1}t$$

$$A_{5,13} = 1/4\hat{J}_{3,2}r + \left(1/4\hat{J}_{3,1} + 3/2\hat{J}_{3,2} + 1/4\hat{J}_{3,3}\right)s + 1/2\hat{J}_{3,2} + 1/4\hat{J}_{3,2}t$$

$$A_{5,15} = 1/4\hat{J}_{1,2}r + \left(1/4\hat{J}_{1,1} + 3/2\hat{J}_{1,2} + 1/4\hat{J}_{1,3}\right)s + 1/2\hat{J}_{1,2} + 1/4\hat{J}_{1,2}t$$

$$A_{5,16} = \left(3/2\hat{J}_{3,1} + 1/4\hat{J}_{3,2} + 1/4\hat{J}_{3,3}\right)r - 1/2\hat{J}_{3,1} + 1/4\hat{J}_{3,1}s + 1/4\hat{J}_{3,1}t$$

$$A_{5,18} = \left(3/2\hat{J}_{1,1} + 1/4\hat{J}_{1,2} + 1/4\hat{J}_{1,3}\right)r - 1/2\hat{J}_{1,1} + 1/4\hat{J}_{1,1}s + 1/4\hat{J}_{1,1}t$$

$$A_{5,19} = \left(-\hat{J}_{3,3} - \hat{J}_{3,2} - 3\hat{J}_{3,1}\right)r + \left(-\hat{J}_{3,3} - 3\hat{J}_{3,2} - \hat{J}_{3,1}\right) s + \left(-3\hat{J}_{3,3} - \hat{J}_{3,2} - \hat{J}_{3,1}\right)t$$

$$A_{5,21} = \left(-\hat{J}_{1,3} - \hat{J}_{1,2} - 3\hat{J}_{1,1}\right)r + \left(-\hat{J}_{1,3} - 3\hat{J}_{1,2} - \hat{J}_{1,1}\right) s + \left(-3\hat{J}_{1,3} - \hat{J}_{1,2} - \hat{J}_{1,1}\right)t$$

$$A_{6,1} = 1/4\hat{J}_{2,3}r + 1/4\hat{J}_{2,3}s + \left(1/4\hat{J}_{2,1} + 1/4\hat{J}_{2,2} + 3/2\hat{J}_{2,3}\right)t - 1/2\hat{J}_{2,3}$$

$$A_{6,2} = 1/4\hat{J}_{1,3}r + 1/4\hat{J}_{1,3}s + \left(1/4\hat{J}_{1,1} + 1/4\hat{J}_{1,2} + 3/2\hat{J}_{1,3}\right)t - 1/2\hat{J}_{1,3}$$

$$A_{6,4} = 1/4\hat{J}_{2,3}r + 1/4\hat{J}_{2,3}s + \left(1/4\hat{J}_{2,1} + 1/4\hat{J}_{2,2} + 3/2\hat{J}_{2,3}\right)t + 1/2\hat{J}_{2,3}$$

$$A_{6,5} = 1/4\hat{J}_{1,3}r + 1/4\hat{J}_{1,3}s + \left(1/4\hat{J}_{1,1} + 1/4\hat{J}_{1,2} + 3/2\hat{J}_{1,3}\right)t + 1/2\hat{J}_{1,3}$$

$$A_{6,7} = 1/4\hat{J}_{2,2}r + \left(1/4\hat{J}_{2,1} + 3/2\hat{J}_{2,2} + 1/4\hat{J}_{2,3}\right)s - 1/2\hat{J}_{2,2} + 1/4\hat{J}_{2,2}t$$

$$A_{6,8} = 1/4\hat{J}_{1,2}r + \left(1/4\hat{J}_{1,1} + 3/2\hat{J}_{1,2} + 1/4\hat{J}_{1,3}\right)s - 1/2\hat{J}_{1,2} + 1/4\hat{J}_{1,2}t$$

$$A_{6,10} = \left(3/2\hat{J}_{2,1} + 1/4\hat{J}_{2,2} + 1/4\hat{J}_{2,3}\right)r + 1/2\hat{J}_{2,1} + 1/4\hat{J}_{2,1}s + 1/4\hat{J}_{2,1}t$$

$$A_{6,11} = \left(3/2\hat{J}_{1,1} + 1/4\hat{J}_{1,2} + 1/4\hat{J}_{1,3}\right)r + 1/2\hat{J}_{1,1} + 1/4\hat{J}_{1,1}s + 1/4\hat{J}_{1,1}t$$

$$A_{6,13} = 1/4\hat{J}_{2,2}r + \left(1/4\hat{J}_{2,1} + 3/2\hat{J}_{2,2} + 1/4\hat{J}_{2,3}\right)s + 1/2\hat{J}_{2,2} + 1/4\hat{J}_{2,2}t$$

$$A_{6,14} = 1/4\hat{J}_{1,2}r + \left(1/4\hat{J}_{1,1} + 3/2\hat{J}_{1,2} + 1/4\hat{J}_{1,3}\right)s + 1/2\hat{J}_{1,2} + 1/4\hat{J}_{1,2}t$$

$$A_{6,16} = \left(3/2\hat{J}_{2,1} + 1/4\hat{J}_{2,2} + 1/4\hat{J}_{2,3}\right)r - 1/2\hat{J}_{2,1} + 1/4\hat{J}_{2,1}s + 1/4\hat{J}_{2,1}t$$

$$A_{6,17} = \left(3/2\hat{J}_{1,1} + 1/4\hat{J}_{1,2} + 1/4\hat{J}_{1,3}\right)r - 1/2\hat{J}_{1,1} + 1/4\hat{J}_{1,1}s + 1/4\hat{J}_{1,1}t$$

$$A_{6,19} = \left(-\hat{J}_{2,3} - \hat{J}_{2,2} - 3\hat{J}_{2,1}\right)r + \left(-\hat{J}_{2,3} - 3\hat{J}_{2,2} - \hat{J}_{2,1}\right) s + \left(-3\hat{J}_{2,3} - \hat{J}_{2,2} - \hat{J}_{2,1}\right)t$$

$$A_{6,20} = \left(-\hat{J}_{1,3} - \hat{J}_{1,2} - 3\hat{J}_{1,1}\right)r + \left(-\hat{J}_{1,3} - 3\hat{J}_{1,2} - \hat{J}_{1,1}\right) s + \left(-3\hat{J}_{1,3} - \hat{J}_{1,2} - \hat{J}_{1,1}\right)t$$

References

Aboudi, J., 1982. A continuum theory for fiber-reinforced elastic viscoplastic composites. Int. J. Eng. Sci. 20, 605–621.

Aboudi, J., 1991. Mechanics of Composite Materials: A Unified Micromechanical Approach. Elsevier, Amsterdam.

Aboudi, J., 2001. Micromechanical analysis of fully coupled electro-magneto-thermo-elastic multiphase composites. Smart Mater. Struct. 10, 867–877.

Aboudi, J., 2004. The generalized method of cells and high-fidelity generalized method of cells micromechanical models – a review. Mech. Adv. Mater. Struct. 11, 329–366.

Aboudi, J., 2005. Micromechanically established constitutive equations for multiphase materials with viscoelastic–viscoplastic phases. Mech. Time-Depend. Mater. 9, 121–145.

Aboudi, J., 2007. Micromechanical analyses of smart composite materials. In: Reece, P.L. (Ed.), Progress in Smart Materials and Structures. Nova Science Publishers, New York, pp. 291–361.

Aboudi, J., 2011. The effect of anisotropic damage evolution on the behavior of ductile and brittle matrix composites. Int. J. Solids Struct. 48, 2102–2119.

Aboudi, J., Freed, Y., 2010. Micromechanical modeling of shape memory alloy composites. In: Chen, H.R. (Ed.), Shape Memory Alloys: Manufacture, Properties and Applications. Nova Science Publishers, pp. 371–423.

Aboudi, J., Pindera, M.-J., Arnold, S.M., 2002. High-fidelity generalized method of cells for inelastic periodic multiphase materials. NASA TM-2002-211469.

Aboudi, J., Pindera, M.-J., Arnold, S.M., 2003. Higher-order theory for periodic multiphase materials with inelastic phases. Int. J. Plasticity 19, 805–847.

Aboudi, J., Arnold, S.M., Bednarcyk, B.A., 2013. Micromechanics of Composite Materials: A Generalized Multiscale Analysis Approach. Elsevier, Oxford, UK.

Bansal, Y., Pindera, M.-J., 2006. Finite volume direct averaging micromechanics of heterogeneous materials with elastic–plastic phases. Int. J. Plasticity 22, 775–825.

Bednarcyk, B.A., Arnold, S.M., 2003. Micromechanics-based modeling of woven polymer matrix composites. AIAA 41, 1788–1796.

Bednarcyk, B.A., Aboudi, J., Arnold, S.M., 2010. Micromechanics modeling of composites subjected to multiaxial progressive damage in the constituents. AIAA J. 48, 1367–1378.

Bednarcyk, B.A., Aboudi, J., Arnold, S.M., Sullivan, R.M., 2008. Analysis of space shuttle external tank spray-on foam insulation with internal pore pressure. J. Eng. Mater. Technol. 130, 041005-16–16.

Bednarcyk, B.A., Arnold, S.M., Aboudi, J., Pindera, M.-J., 2004. Local field effects in titanium matrix composites subject to fiber-matrix debonding. Int. J. Plasticity 20, 1707–1737.

Christensen, R.M., 1979. Mechanics of Composite Materials. Wiley-Interscience, New York.

Eshelby, J.D., 1957. The determination of the elastic field of an ellipsoidal inclusion, and related problems. Proc. R. Soc. A 241, 376–396.

Fish, J., Yu, Q., Shek, K., 1999. Computational damage mechanics for composite materials based on mathematical homogenization. Int. J. Numer. Methods Eng. 45, 1657–1679.

Gavazzi, A.C., Lagoudas, D.C., 1990. On the numerical evaluation of Eshelby's tensor and its application to elastoplastic fibrous composites. Comput. Mech. 7, 13–19.

Haj-Ali, R.M., 2009. Cohesive micromechanics: a new approach for progressive damage modeling in laminated composites. Int. J. Damage Mech. 18, 691–719.

Haj-Ali, R., Aboudi, J., 2009. Nonlinear micromechanical formulation of the high fidelity generalized method of cells. Int. J. Solids Struct. 46, 2577–2592.

Haj-Ali, R., Aboudi, J., 2010. Formulation of the high-fidelity generalized method of cells with arbitrary cell geometry for refined micromechanics and damage in composites. Int. J. Solids Struct. 47, 3447–3461.

Haj-Ali, R., Aboudi, J., 2012. Discussion paper: has renaming the high fidelity generalized method of cells been justified? Int. J. Solids Struct. 49, 2051–2058.

Haj-Ali, R., Kilic, H., Zureick, A.H., 2001. Three-dimensional micromechanics-based constitutive framework for analysis of pultruded composite structures. J. Eng. Mech. 127, 653–660.

Hori, M., Nemat-Nasser, S., 1993. Double-inclusion model and overall moduli of multiphase composites. Mech. Mater. 14, 189–206.

Jain, J.R., Ghosh, S., 2008. Homogenization based 3D continuum damage mechanics model for composites undergoing microstructural debonding. J. Appl. Mech. 75. http://dx.doi.org/10.1115/1.2870265.

Jain, J.R., Ghosh, S., 2009. Damage evolution in composites with a homogenization-based continuum damage mechanics model. Int. J. Damage Mech. 18, 533–568.

Ju, J.W., Sun, L.Z., 2001. Effective elastoplastic behavior of metal matrix composites containing randomly located aligned spheroidal inhomogeneities. Part I: Micromechanics-based formulation. Int. J. Solids Struct. 38, 183–201.

Ju, J.W., Tseng, K.H., 1996. Effective elastoplastic behavior of two-phase ductile matrix composites: a micromechanical framework. Int. J. Solids Struct. 33, 4267–4291.

Levy, A., Papazian, J.M., 1990. Tensile properties of short fiber-reinforced SiC/Al composites: finite-element analysis. Metall. Trans. 21A, 411–420.

Liu, K.C., Chattopadhyay, A., Bednarcyk, B.A., Arnold, S.M., 2011. Efficient multiscale modeling framework for triaxially braided composites using generalized method of cells. J. Aerosp. Eng. 24, 162–170.

Mori, T., Tanaka, K., 1973. Average stress in matrix and average elastic energy of materials with misfitting inclusions. Acta Metall. 21, 571–574.

Muliana, A.H., Kim, J.S., 2007. A concurrent micromechanical model for predicting nonlinear viscoelastic responses of composites reinforced with solid spherical particles. Int. J. Solids Struct. 44, 6891–6913.

Pahr, D.H., Arnold, S.M., 2002. The applicability of the generalized method of cells for analyzing discontinuously reinforced composites. Compos. Part B 33, 153–170.

Paley, M., Aboudi, J., 1992. Micromechanical analysis of composites by the generalized cells model. Mech. Mater. 14, 127–139.

Paulino, G.H., Yin, H.M., Sun, L.Z., 2006. Micromechanics-based interfacial debonding model for damage of functionally graded materials with particle interactions. Int. J. Damage Mech. 15, 267–288.

Ryvkin, M., Aboudi, J., 2007. The effect of fiber loss in periodic composites. Int. J. Solids Struct. 44, 3497–3513.

Wang, Y.M., Weng, G.J., 1992. The influence of inclusion shape on the overall viscoelastic behavior of composites. J. Appl. Mech. 59, 510–518.